Field gamma dose-rate measurement with a NaI(Tl) detector: re-evaluation of the "threshold" technique

N. Mercier[1] and C. Falguères[2]

1. Laboratoire des Sciences du Climat et de l'Environnement-IPSL, UMR CEA-CNRS-UVSQ, Domaine du CNRS, Avenue de la Terrasse, 91198 Gif-sur-Yvette Cedex, France

2. Département de Préhistoire du Muséum National d'Histoire Naturelle de Paris, 1 rue René Panhard, 75013 Paris, France

(Received 27 September 2006; in final form 7 May 2007)

Abstract

Radiation detectors, like doped NaI, are commonly used in the field for the determination of gamma dose-rates. In most cases, and even though these systems generally allow one to record the full gamma spectrum between 0 to around 3 MeV, this dose-rate is computed from the count rates recorded in a limited number of "windows" (Aitken, 1985). With this technique, only a small part of the spectrum is therefore exploited. Nevertheless, an alternative approach - the "threshold" technique – known for more than 30 years, can easily be used with the same detection system. In this paper, we make a re-evaluation of this technique and discuss its limits and advantages.

Introduction

In a paper published in 1974, Løvborg and Kirkegaard investigated the response of a 3 inch by 3 inch NaI(Tl) detector placed above environments of known radioactivity. According to their experimental and theoretical results for this 2π geometry, the count-rate of their equipment above a chosen threshold (370 keV) was found to be directly proportional to the gamma dose-rate. As the gamma rays come from the radioactive elements of the U- and Th-series and from the ^{40}K, this means that the count-rate was independent of these three sources.

In the next years, Murray, Bowman and Aitken (1978) developed a portable system equipped with a NaI(Tl) detector for gamma dose-rate measurements; it is discussed in Aitken (1985, p. 107-108) as the "gamma scintillometer". In their experiments, they inserted their detector in radioactive doped blocks set up at the Research Laboratory for Archaeology and the History of Art (see Rhodes and Schwenninger, 2007). With these experimental conditions, which are close to field conditions, they concluded that a threshold value could also be defined for their equipment (at 450 keV). However, these authors showed that this threshold occurred in a region of the spectrum where the count-rate changed rapidly with energy, and they then emphasized the necessity to stabilize the system to account for temperature variations.

We recently tested this approach with a 1.5 inch by 1.5 inch NaI(Tl) detector (IPRON-1 connected to a multichannel analyser: Inspector1000 – Canberra) and report here our results and conclusions.

General

In luminescence and ESR dating, the gamma dose-rate generally constitutes a significant component of the total dose-rate and has to be determined precisely. This dose-rate can be measured directly with synthetic dosimeters (e.g. Al_2O_3:C or $CaSO_4$:Dy) buried for relatively long periods of time (weeks or even months), or by inserting in the sediment a portable detector connected to a spectrometer and recording the gamma spectrum. In this case, the gamma dose-rate is calculated from the radioisotopic contents of the sediment (U, Th and K) determined by the "classical" technique, which is based on the definition of three regions of interest ("windows"), each window being centred on a gamma ray energy specific to an isotope (1460 keV for ^{40}K; 1780 keV for ^{214}Bi (U-series) and 2620 keV for ^{208}Tl (Th-series), see for instance Aitken (1985, p.102-105). In each of these two last windows, the counting is due to the detection of gamma rays coming from both the U- and Th-series, whereas in the "K window" the three sources contribute. Mathematically, one can then simply write for each window the following equation:

$$N = n_K . [K] + n_U . [U] + n_{Th} . [Th]$$

where the total count N (per unit of time) is the sum of three factors in which [K], [U] and [Th] are the radioisotopic contents of the sediment and n_K, n_U and n_{Th} represent the detection efficiencies of the detector in the considered window for the three sources. These efficiency factors are then expressed as the number of counts per unit of time for 1 ppm (for the U- and Th-series) and 1% for K.

In considering the threshold approach, these factors have to be interpreted as the number of counts per unit time for 1 µGy/a and [K], [U] and [Th] as the gamma dose-rates in the sediment. Consequently, for N to be proportional to the total dose-rate, n_K, n_U and n_{Th} must have the same value n. In this case, the above equation can be written as :

$$N = n \cdot ([K] + [U] + [Th])$$

where ([K] + [U] + [Th]) is the total gamma dose-rate.

In practice, for using this approach with a given detector, one has simply to define the energy for which the values of n_K, n_U and n_{Th} are identical.

Experiments

One way to answer this question is to get "pure" spectra taken in environments containing only one source of radioelements (either K, U- or Th-series). Such environments do not naturally exist, so we used the doped blocks set up at the Research Laboratory for Archaeology and Art, in Oxford, as reported by Murray et al. (1978). These blocks made of concrete were doped with uranium, thorium and potassium and provide the following gamma dose-rates: U-block: 13.27 Gy/ka; Th-block: 7.10 Gy/ka; K-block: 1.38 Gy/ka. A non-doped block made of the same concrete is also available and is used as a background standard with a gamma dose-rate of 0.53 Gy/ka (Rhodes and Schwenninger, 2007). According to these authors, the Th-block contains a small portion of U with a U/Th ratio of 0.043. Considering this ratio and the dose-rate conversion factors given by Adamiec and Aitken (1998), one can calculate the effective radioisotope concentrations : U-block (117.4 ppm), Th-block (135.2 ppm of Th and 5.8 ppm of U), K-block (5.7 %).

Note that these values are slightly different from those given in Rhodes and Schwenninger (2007) since they used the conversion factors of Nambi and Aitken (1986).

Fig. 1 shows the spectra recorded with our gamma probe. After time normalisation (1 ksec), "pure" spectra were calculated by subtracting the signal measured in the non-doped block (thus including the background of the detector and the cosmic contribution) and were normalised to 1 ppm of U or Th, and 1 % of K (Fig. 2), by using the effective radioisotope concentrations cited above. This step was necessary in order to subtract from the Th spectrum the small contribution from U present in the Th-block.

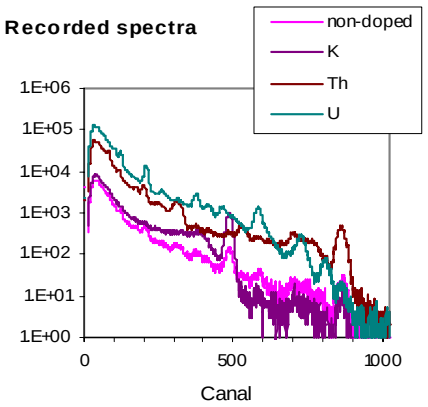

Figure 1: *Spectra recorded with the NaI(Tl) probe in the four Oxford blocks. The multichannel analyser was configured for recording 1024 channels. Measurement times were about 35 minutes for the U, Th and K-doped blocks, and 1.1 hour for the non-doped block. Energy calibration of each spectrum was carried out by identifying specific gamma rays.*

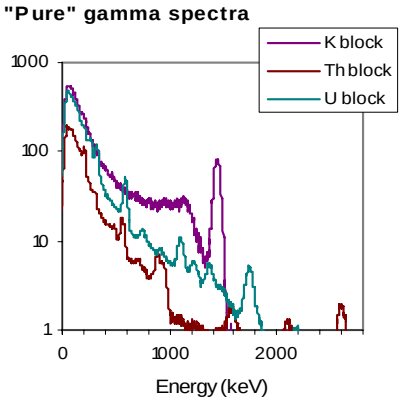

Figure 2: *Spectra given as the number of counts per 1000 seconds and 1 ppm (for U and Th) or 1% (for K) after subtraction of the spectrum recorded in the non-doped block. Notice that for the K spectrum, the contribution of the concrete was limited to 72% due to its dilution by the added potassium salt. A correction was also applied to the Th spectrum for taking into account the uranium contamination (5.8 ppm) present in the Th block. Note that the U, Th and K contents of blocks were deduced from dose measurements performed with dosimeters (Rhodes and Schwenninger, 2007) and differ slightly from the values used by Murray et al. (1978).*

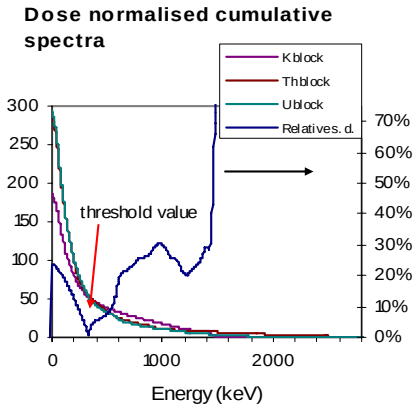

Figure 3: *Cumulative spectra as a function of energy deduced from Fig. 2. For any x-value, the y-axis indicates the number of counts above this energy. Each spectrum was dose normalised according to the gamma conversion factors given by Adamiec and Aitken (1998). The right axis gives the relative standard deviation of the three cumulative spectra; the minimum value is around 320 keV.*

To define the threshold for our detector, these pure spectra were normalised with the dose-rate conversion factors given by Adamiec and Aitken (1998) and thereafter cumulative spectra were computed (Fig. 3). For any given energy, the left y-axis value is the total count recorded by the detector for the corresponding source (either U-series, Th-series or K). The three spectra have a similar shape and are close to each other in the 200-600 keV energy range. By computing the standard deviation of these curves as a function of energy (right y-axis on Fig. 3), the minimum value appears to be located around 320 keV. Hence, for this particular energy value, the n_U, n_{Th} and n_K parameters are almost identical : the n factor of our detector is 53.7 counts/ 1 ksec/ 1 µGy/a.

Testing the "threshold" approach

We tested this approach by recording a gamma spectrum in a block made of building bricks available at the Gif laboratory (Mercier et al., 1994). The radioisotopic contents of these bricks produced in the Auvergne region (France) were determined by NAA and high resolution gamma spectrometry and are, on average : U 6.40±0.68 ppm; Th 22.89±2.43 ppm; K 3.61±0.23 %. These analyses indicated no disequilibrium in the U- or Th-series. A $CaSO_4$:Dy dosimeter placed at the centre of this block recorded a dose-rate to quartz of 2578±80 µGy/a – corrected for a small cosmic contribution estimated at 160 µGy/a after Prescott and Hutton (1994). The gamma dose-rate deduced from the "threshold" approach using the NaI detector (2475 µGy/a) was found to be in good agreement with this value.

Here, an important point is to estimate the error associated with the calculated value. At least three sources have to be studied: counting statistics, disequilibrium in the radioelement series, and energy calibration.

1) The gamma spectrum recorded in the Gif block was taken using a counting time of 1342 seconds and the number of counts above the threshold was 186,980; the counting statistics were then sufficient to ensure that they do not constitute the main source of error. Notice that the threshold factor (53.7 counts/ 1 ksec/ 1 µGy/a) allows one to estimate easily the contribution of the statistics to the total error or, for an accepted error, to evaluate the minimum time of counting (if one has a rough estimation of the dose-rate in the sediment). For instance, for a sediment with a gamma dose-rate of about 500 µGy/a, a counting time of 5 minutes is sufficient to get a counting precision around 1%.

2) As noted above, the U- and Th-series are in secular equilibrium in the Gif block. It was assumed that this situation prevails also in the Oxford blocks, and this is indirectly confirmed by the test done in the Gif block. However, if one of the doped blocks, for instance the U block, exhibited strong radioactive disequilibrium because of radon loss, one would expect that the U cumulative spectrum of Fig. 3 would have a slightly different shape since post-radon emitters give high energy gamma rays: such disequilibrium would therefore have a small impact on the calibration as the value of the threshold would stay virtually unchanged. Moreover, it is important to recall here that the threshold approach takes account of most of the emitted gamma rays and should be a little bit less sensitive to radioactive disequilibrium than the classical windows technique, from which the U content is derived from the ^{214}Bi gamma ray (1780 keV), detected in the U window, i.e. a post ^{222}Rn emitter.

3) The main source of error is probably related to the energy calibration of a recorded spectrum, and consequently, to the setting of the threshold for this spectrum. For this purpose, one can generally use the ^{40}K peak at 1460 keV but it can also be useful to have at hand, especially if the counting time is reduced to a few minutes, a short-lived radioactive element (such as ^{133}Ba which has multiple gamma ray lines under 500 keV, or ^{241}Am as discussed in Aitken (1985, p. 323-324)). Such a source can be used just before and after recording the spectrum in the sediment. It should be noted that it is illegal to carry such a source

on an aeroplane. In some gamma spectrometers (e.g. Harwell Nutmaq) such a source was built in to the detection head in order to overcome energy drift with changing temperature.

To estimate the influence of the calibration on the deduced dose-rate, we computed this dose-rate in the interval 300-360 keV (as we estimate that the energy calibration can be performed with a maximum error of ±30 keV). The deduced values would vary from 2422 to 2481 µGy/a with a minimum of 2414 µGy/a at 310 keV. According to this example, one can therefore estimate that the error introduced by the energy calibration of the spectrum is less than 3% for our detector.

Conclusions

By using a large part of the spectrum (all the counts above a fixed energy), the "threshold" approach allows one to reduce considerably the recording time and this limits the undesirable effects of temperature changes during measurement. In considering the different sources of error, including the accuracy of the gamma dose-rates measured in the Oxford blocks, one can estimate the overall error associated with a dose determination to be around 5 %. In spite of these encouraging results, it seems important to make systematic comparisons with doses recorded with dosimeters, especially by choosing different environments (dominated by silicates, carbonates, clays, or others) in order to study their influence on the threshold value (see Liritzis and Galloway, 1980).

Furthermore, as this approach makes use of a large part of the spectrum (in contrast with the "windows" technique), it is tempting to reduce the size of the detector for use in sediments rich in stones or gravels and also in archaeological layers. Also, the resolution of the detector is not a critical parameter with the threshold approach, neither is the light output efficiency relative to NaI, and other crystals could then be tested.

Acknowledgements

The authors wish to thank J.-L. Schwenninger for his help during the recording of the spectra, A.G. Wintle and G.A.T. Duller for their advice and A.S. Murray for his helpful comments on an earlier version of this paper.

References

Adamiec, G. and Aitken, M. J. (1998). Dose-rate conversion factors: update. *Ancient TL*, **16**, 37-50.

Aitken, M. J. (1985). *Thermoluminescence dating.* Academic Press, London.

Liritzis, Y. and Galloway, R. B. (1980). A new technique for calibrating a NaI(Tl) scintillometer used to measure gamma dose-rates in archaeological sites. *Nuclear Instruments and Methods*, **174**, 593-597.

Løvborg, L. and Kirkegaard, P. (1974). Response of 3" x 3" NaI(Tl) detectors to terrestrial gamma radiation. *Nuclear Instruments and Methods*, **121**, 239-251.

Mercier, N., Valladas, H. and Valladas, G. (1994). A new dosimetric calibration tool. *Nuclear Tracks and Radiation Measurements*, **23**, 507-508.

Murray, A. S., Bowman, S. G. E. and Aitken, M. J. (1978). Evaluation of the gamma dose-rate contribution. *PACT* **2**, 84-96.

Nambi, K.S.V. and Aitken, M.J. (1986). Annual dose conversion factors for TL and ESR dating. *Archaeometry* **28**, 202-205.

Prescott, J.R. and Hutton, J.T. (1994). Cosmic ray contributions to dose rates for luminescence and ESR dating: large depths and long-term variations. *Radiation Measurements*, **23**, 497-500.

Rhodes, E. and Schwenninger, J-L. (2007). Dose rates and radioisotope concentrations in the concrete calibration blocks at Oxford. *Ancient TL*, **25**, 5-8.

Reviewer

A.S. Murray

Dose rates and radioisotope concentrations in the concrete calibration blocks at Oxford

E.J. Rhodes[1] and J.-L. Schwenninger[2]

1. Research School of Earth Sciences and Research School of Asian and Pacific Studies, The Australian National University, Canberra, ACT 0200, Australia (Ed.Rhodes@anu.edu.au)
2. Research Laboratory for Archaeology & the History of Art, University of Oxford, Dyson Perrins Building, South Parks Road, Oxford, OX1 3QY, UK

(Received 21 Nov 2006; in final form 22 May 2007)

Introduction

The "Oxford Blocks" were constructed for the calibration of portable gamma spectrometers, and consist of 4 concrete cubes measuring 50 cm along each edge, each with a central horizontal cylindrical hole of 11.0 cm diameter which goes from one side to the other. Three blocks have material added to increase their radioactivity; the U block includes ground pitchblende, the Th block contains monazite sand and the K block has a potassium-bearing salt (sulphate of potash) mixed with the concrete, to provide calibration standards for U, Th and K respectively. The fourth block is plain concrete, and acts as a background standard. They are suitable for the calibration of portable gamma spectrometers with probes up to 3 inches in diameter. They are separated from each other by additional plain concrete blocks without holes, to reduce crosstalk between blocks during measurements. Each calibration block has additional concrete cylinders which reside within the central holes; two 25 cm lengths each comprise three cylinders which fit inside each other, made of the same concrete mix as their respective block. One set of three cylinders is removed during spectrometer calibration, and the remaining set adjusted to allow the detection crystal to be central; that is the centre of the crystal is positioned 25 cm from both front and back faces. The K block contains only 72% concrete, the rest being sulphate of potash, and the monazite sand in the Th block contains a small amount of U; these must be taken into account during the calibration process.

The blocks were constructed in 1973 (Bowman, 1976) to the rear of the Research Laboratory for Archaeology and the History of Art (RLAHA), 6 Keble Road, Oxford, UK. After construction, neutron activation analysis (NAA) and thick-source alpha counting of small sub-samples were used to derive preliminary radioisotope concentrations. Partly to overcome concerns that the radioisotopes might not be distributed evenly, the gamma dose rates in each block were subsequently measured directly using TL dosimeters; it is these measurements from which the quoted dose rate values, and estimated radioisotope concentrations, are derived (Table 1).

Block dose rate determinations

In 1973, dose rate determinations were made by placing small copper capsules containing heated natural CaF_2 (calcium fluoride) grains in each block for a period of several months, and measuring the acquired dose using TL measurements. This procedure was regularly repeated by RLAHA students (Gaffney, Clark and Rhodes) until around 1989, using a calibrated $^{90}Sr/^{90}Y$ source and a regenerative-dose procedure on equipment in the main glow room in Oxford. Martin Aitken treated the CaF_2 by light exposure prior to its placement in the copper capsules in order to reduce sensitivity change during TL measurement.

The dose rate determination procedure was as follows. TL estimates of dose were made using capsules containing CaF_2 placed in all four blocks, K, U, Th and background (BG) blocks for a known time, typically around 3 months. After heating the capsules in order to zero the TL signal, they were placed at the geometric centre of each block, and the moveable concrete cylinders arranged to minimize voids around each capsule. At the end of the exposure period, the capsules were opened in turn, and the dose determined for each using a simple single aliquot regenerative-dose TL procedure; two or three aliquots were measured for each block and the mean values used in calculations. The total measured dose rate values from the U, Th and K blocks had the measured concrete, and estimated cosmic and self dose rates subtracted. Note that for the K block, only 72% of the BG block concrete component is subtracted since the sulphate of potash used to dope the concrete constitutes 28% of the block. These

	K block	Th block	U block	BG block
Concrete	72%	~100%	~100%	~100%
Gross dose rates (mGy/a)	1.75	7.05	12.66	0.60
Concrete, self dose, cosmic (mGy/a)*	0.50	0.60	0.60	0.60
Net dose rate (mGy/a)	1.25	6.45	12.06	0.00
Wall corrected (x1.1) (mGy/a)	**1.38**	7.10	**13.27**	-
Th dose rate, Th block (92.3%) (mGy/a)	-	**6.55**	-	-
U dose rate, Th block (7.7%) (mGy/a)	-	**0.55**	-	-
Effective concentrations, using Nambi and Aitken (1986)	5.71% K	125.7 ppm Th 4.8 ppm U	116.8 ppm U	

Note :
* The K block is only 72% concrete, and this must be taken into consideration when subtracting the background block dose rate, which comprises contributions from concrete, and estimated self dose (0.1 mGy/a) and cosmic dose rate (0.16 mGy/a). The Th block contains a small amount of U; Th and U dose rates are estimated based on the certified Th:U ratio. Note that these values only represent "excess" dose rates; values in bold represent the current best estimates of dose rates for the Oxford Blocks.

Table 1: *Effective dose rates and concentrations of K, U and Th in the Oxford concrete calibration blocks. These were measured directly using TL of calcium fluoride in copper capsules. The values in this table represent a combination of measurements made by Gaffney (1983), Clark (1984) and Rhodes (1985-89).*

"excess" values (that is, the dose rate contributions only from the added materials in each block) were then corrected for capsule wall attenuation, using a correction factor of 1.1 for the 1 mm copper wall.

As mentioned above, a small contribution to the gamma dose rate in the Th block is from U, which represents an integral part of the natural monazite sand used. The U:Th concentration ratio for this sand was quoted as 0.035 by NBL on the original certification (Martin Aitken, unpublished notes), and this value was used to apportion the measured dose rate to U and Th using dose rate conversion factors. We note that this concentration ratio has more recently been determined using NAA by EJR as 0.043. In principle, this ratio could also be determined using a calibrated NaI spectrometer, or by high resolution Ge spectra of the same monazite sand.

This procedure yields net dose rate values for each block which are used in the calibration of gamma spectrometers to derive individual U, Th and K dose rates from subsequent field measurements, and also for the calculation of total dose rate using the threshold method. For this reason, these effective "excess" dose rates are of primary importance, rather than the U, Th and K concentrations calculated using conversion factors. However, the values that have previously been widely quoted for the blocks are expressed as "effective concentrations" of K, U and Th, estimated using either Nambi and Aitken (1986) or with earlier conversion factors.

The dose rate values presented in Table 1 represent estimates based on combined measurements by Chris Gaffney (in 1983), Peter Clark (in 1984) and Ed Rhodes (1985 to 1989), and represent an update on the values given by Aitken (1985; appendix L). Also shown are the widely circulated radioisotope concentration values (note that the potassium concentration quoted here as 5.71% K is equivalent to 6.88% K_2O).

Discussion
The process described above for characterising the blocks for use as calibration standards relies on several assumptions, namely:

1. CaF_2 provides an accurate estimate of dose-rate on timescales of months,
2. the background dose-rate subtraction does not introduce error,
3. the correction for copper capsule wall attenuation is accurate,
4. the laboratory beta source calibration is accurate,
5. the size of blocks is sufficient for good replication of an infinite matrix,

and for accurate radioisotope concentrations,

6. the dose-concentration conversion factors used are accurate.

The use of CaF_2 in copper capsules to determine small environmental doses has been standard practice for many years (e.g. Aitken 1985), and is not discussed further here. As the dose rate measured in the concrete background block is subtracted from the gross dose rates for the U and Th blocks, it is not important what the relative magnitude of the concrete, self dose and cosmic dose rates are. However, this does matter a little for the K block which is only 72% concrete; we consider that the cosmic dose rate is probably underestimated, and we have no information regarding the CaF_2 self dose rate. For the derivation of the dose rates presented in Table 1, a single wall correction factor of 1.1 was used irrespective of the gamma energies present, for the 1mm thick copper capsule. We consider that there may be room to improve this value in the future using modern Monte-Carlo modelling (e.g. Nathan et al., 2003), and Al_2O_3:C may represent an improved material for future dose rate assessments (e.g. Burbidge and Duller 2003).

The RLAHA beta source calibration was undertaken on several occasions, notably by Bert Roberts and Nigel Spooner in 1993. It was re-assessed by Phil Toms using a SAR OSL protocol in 1998, who demonstrated agreement within 1% for calibrations based on irradiations at GSF (Munich, Germany), NIST (Gaithersburg, USA) and the NPL (UK). Note that the K, U and Th concentration values which are widely circulated and presented below in Table 1 rely on the energy conversion values of Nambi and Aitken (1986). The updated values of Adamiec and Aitken (1998) provide improved estimates and these are given in Mercier and Falguères (2007).

Whether the blocks are of sufficient size to replicate the geometry used for in-situ gamma measurements has been a matter of debate. Jean Fain expressed concern, in particular for the Th block, for which the ^{208}Tl emission at 2614.6 keV represents the line used in NaI spectrometry for Th concentration estimation. If this block is too small to reproduce the full spectrum of infinite matrix Th emissions accurately, the estimated effective concentration will differ slightly from the true concentration. The effect will be greater for higher energy gamma emissions, which travel further through the concrete matrix. However, the estimation of total dose rate will not be severely affected, as this relies on the direct measurement of a luminescence dose using CaF_2, which includes contributions across the full energy spectrum. In summary, the calibration of the gamma spectrometry estimation of Th content using the 2614.6 keV ^{208}Tl emission will be the parameter most influenced by non-infinite matrix effects caused by the limited block size. The estimated Th content using spectrometers calibrated in these blocks, should consequently be treated with some caution, while the total Th series gamma dose rate contribution remains relatively well determined. The same effect, though to a reduced magnitude, is expected for the K and U blocks.

Gamma dose rate data collected with an EG&G MicroNomad NaI portable spectrometer, which was calibrated in these blocks using the values shown in Table 1, were used in the relatively high precision OSL age estimates of archaeological sediments presented by Rhodes et al. (2003). Very good agreement with radiocarbon dating was observed, with no indication of any systematic error; beta dose rates were calculated using NAA determination of K, U and Th content. The ratio of the mean sediment K and U contents determined by NaI and NAA was within 5% of unity, while for Th the mean of the NaI to NAA ratio was 0.90 ± 0.06. These observations are consistent with the expectations discussed above, namely that the gamma dose rate contributions should be well estimated, but that individual concentrations of K, U and Th are probably less reliable, in particular the Th value.

The blocks were recently relocated from the Keble Road site to the rear of the Dyson Perrins Laboratory in specially constructed steel cradles, where their original relative geometry is retained. It now seems sensible to update the dose rate estimates with new measurements based on Al_2O_3:C.

References

Adamiec, G. and Aitken, M.J. (1998). Dose-rate conversion factors: update. *Ancient TL* **16**, 37-50.

Aitken, M.J. (1985). *Thermoluminescence Dating*. Academic Press, London.

Bowman S.G.E. (1976). *Thermoluminescent dating: the evaluation of the radiation dosage.* Unpublished D.Phil. thesis, University of Oxford.

Burbidge, C.I. and Duller, G.A.T. (2003). Combined gamma and beta dosimetry, using Al_2O_3:C, for in situ measurements on a sequence of archaeological deposits. *Radiation Measurements* **37**, 285-291.

Mercier, N. and Falguères, C. (2007) Field gamma dose-rate measurement with a NaI(Tl) detector: re-evaluation of the "threshold" technique. *Ancient TL* **25**, 1-4.

Nambi, K.S.V. and Aitken, M.J. (1986). Annual dose conversion factors for TL and ESR dating. *Archaeometry* **28**, 202-205.

Nathan, R.P., Thomas, P.J., Jain, M., Murray, A.S. and Rhodes, E.J. (2003). Environmental dose rate heterogeneity of beta radiation and its implications for luminescence dating: Monte Carlo modelling and experimental validation. *Radiation Measurements* **37**, 305-313.

Rhodes, E.J., Bronk-Ramsey, C., Outram, Z., Batt, C., Willis, L., Dockrill, S. and Bond, J. (2003). Bayesian methods applied to the interpretation of multiple OSL dates: high precision sediment age estimates from Old Scatness Broch excavations, Shetland Isles. *Quaternary Science Reviews* **22**, 1231-1244.

Reviewer

A.S. Murray

Editor's Comments

I am very grateful to the authors for putting this paper together, and think that it is very important that the basis for these calibration values have been described. Rhodes and Schwenninger refer in this paper to the DPhil thesis of Sheridan Bowman that was completed in 1976. With the permission of the Sheridan Bowman, a PDF of Appendix A5 of Bowman (1976) is available via the Ancient TL website (http://www.aber.ac.uk/ancient-tl/issue25_1/bowman.pdf). This appendix describes the original construction of the doped concrete blocks in Oxford, and a suite of CaF_2 dosimetry measurements that were made to assess the gamma dose rates in each of them. The gamma dose rates presented in this appendix are different to those given above by Rhodes and Schwenninger, and this perhaps serves to reinforce the final comment in the paper that the gamma doses should be reassessed. Additional information about the original characterisation of these blocks and about construction of a larger U doped block can be found in Murray (1981).

Murray A.S. (1981). *Environmental radioactivity studies relevant to thermoluminescence dating.* Unpublished D.Phil. thesis, University of Oxford.

A note on estimating the error when subtracting background counts from weak OSL signals

Bo Li

Department of Earth Sciences, The University of Hong Kong, Pokfulam Road, Hong Kong, China

(Received 15 March 2007; in final form 26 April 2007)

Abstract
The counting statistics of the instrumental background that underlies all OSL measurements was investigated and found not to follow a Poisson distribution. However, if the instrumental background is assumed to have a Poisson distribution, substantial underestimation of the error of the background-corrected OSL signal may occur, especially for samples with a weak OSL signal. An alternative method is suggested for estimating the error on the background-corrected OSL signal by making a separate measurement of the variance of the instrumental background.

Keywords: error, OSL, counting statistics, Poisson distribution

Introduction

Appropriate estimation of the error for the background-subtracted optically stimulated luminescence (OSL) signal is important for assessing the error of the age calculated in optical dating. The error in the OSL signal is commonly calculated by assuming a Poisson distribution (e.g. Galbraith et al., 1999). Based on this assumption, a formula for calculating the error in the background-corrected OSL signal was proposed by Banerjee et al. (2000). A correction of this formula and more detailed discussion related to the variance calculation for background-corrected OSL signals were given later by Galbraith (2002). In both reports, the OSL signal was assumed to consist of only two components, the initial OSL signal and a constant instrumental background. The error calculation formula was derived by assuming that both the OSL signal and the background follow a Poisson distribution. Although some cases where the background is over-dispersed have been discussed (Galbraith et al., 1999; Galbraith, 2002), the reasons for over-dispersion of the background are still not clear.

Several studies suggest that the OSL signal from quartz actually consists of several components, namely the fast, medium and slow components (e.g. Smith and Rhodes, 1994; Bailey et al., 1997). In continuous-wave OSL (CW-OSL) measurement, the initial part of the signal that is commonly used for dating comes mainly from the fast component and some of the medium component, and the signal in the final part of the decay curve comes mainly from the slow component and the instrumental background (e.g. Li and Li, 2006); the latter is composed of the instrumental noise and scattered light. The slow component and instrumental background are considered to be constant throughout the optical stimulation and are estimated from the final part of the OSL curve. They are subtracted from the initial signal to obtain the background-corrected signal. Hence, the background described in Galbraith et al. (1999) is actually the sum of the instrumental background and the slow component.

Because the intensity of the slow component may vary from sample to sample, the relative contributions of the slow component and the instrumental background to the last part of the OSL signal also vary from sample to sample. Hence, simply assuming that the slow component and background have the same distribution may lead to incorrect estimation of the uncertainty. Thus the variances of the slow component and background observed in the final part of the OSL curve need to be considered separately and incorporated into the error calculation for the background-subtracted signal. This paper aims to investigate whether assuming that the instrumental background has a Poisson distribution is appropriate, and how this assumption would influence the error calculation.

Samples and analytical facilities

The OSL decay curves used in this study were obtained from the quartz extracts of several sediments from China, C5, Wgs1, TWC and DGF-1, used for optical dating. These samples have different initial OSL count rates, ranging from 10^2 to 10^5 cts/s. For OSL measurement, the mineral grains were mounted on 10-mm diameter and 0.5-mm thick aluminum discs with Silkospray silicone oil.

	Disc Number						
	1	2	3	4	5	6	Average
Mean counts (counts/0.2s)	12.9	12.9	12.8	12.7	13.6	12.9	13.0±0.1
Variance (counts/0.2s)^2	25.4	26.3	25.4	26.6	29.5	30.1	27.2±0.9
Variance/Mean	2.0	2.0	2.0	2.1	2.2	2.3	2.1±0.1

Table 1: *The mean counts, variance and variance/ mean ratio of the instrumental background measurement of six aliquots with annealed quartz grains. The aliquots were measured under the same conditions as in OSL measurement (125°C for 100 s with 50% of the maximum power of the blue LEDs).*

All measurements were performed using an automated Risø TL/OSL DA-15 reader equipped with excitation units containing blue light-emitting diodes (LEDs, 470 ± 30 nm) (Bøtter-Jensen et al., 1999). The OSL signal was detected by a photomultiplier tube (PMT) (EMI9235QA) observing the sample through 7.5 mm thickness of U-340 filters. All OSL measurements were carried out at 125°C using blue LEDs with 50% of the maximum power (~30 mW/cm^2).

Results

Variability of the instrumental background

In order to test the variability of the background, some quartz grains extracted from these samples were annealed at 900°C for 2 hours to remove all the OSL signals. The grains were then mounted on six aluminum discs and optically stimulated using the same experimental conditions as those used in practical OSL measurements, i.e. the same stimulation light power and time, and the same holding temperature (125°C). The recording time per channel is the same as that used in OSL measurements (0.2s/channel in this paper). Because all the OSL signals have been removed by annealing, the observed counts should represent the instrumental background.

A typical background as a function of stimulation time from one of the aliquots (disc 6 in Table 1) is shown in Fig. 1. The background is independent of stimulation time with a mean count rate at 12.9 cts/0.2 s, and for the 500 channels shown the standard error is 0.2 cts/0.2 s. The variance is 30.1 (cts/0.2 s)^2 for the data set. A summary of the mean, variance and variance/mean ratio from the six aliquots, and the average of the values obtained are shown in Table 1. There is little difference of mean, variance and variance/mean ratio among the different aliquots, suggesting that the instrumental background and its distribution are similar under specified experimental conditions. The ratio of the variance/mean is 2.1 ± 0.1, rather than 1 as would be expected in the case of a Poisson distribution (e.g. Galbraith, 2002), suggesting that the background is over-dispersed. It should be noted that the variance/mean ratio only changes negligibly if the total counts in successive n (n>1) channels are analysed because the mean counts and the variance would increase proportionally with the integration time. For example, for 5 successive channels (integration time is 1 second), the mean count rate for the data set shown in Fig. 1 in 5 channels is 64 cts/s and the variance is 152 (cts/s)^2, which are all 5 times the values obtained when 1 channel was analysed (Table 1). The variance/mean is 2.4, similar to the value of 2.3 when successive channels (0.2 s) are analysed.

It should be remembered that in some instrumental systems there is electronic division of the signal by a factor of 2; this means that the true variance is 4 times the observed variance and the true count rate is twice the observed one. Therefore, in this case, the observed variance/mean ratio is actually underestimated by a factor of 2, although the relative standard error will not be affected. For this study, the true variance/mean ratio should thus be double the observed one, i.e. 4.2, which is still a strong indication of over-dispersion.

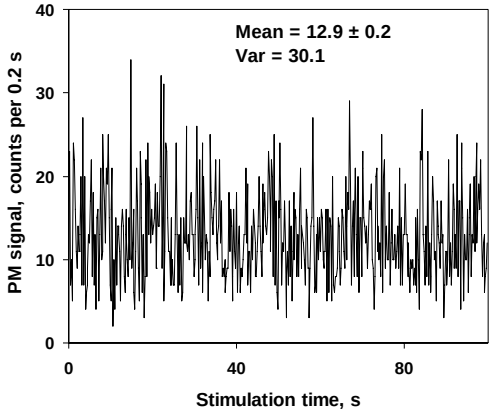

Figure 1: *Typical background signal from annealed quartz grains mounted on an aluminum disc, which was measured under the same conditions as normal OSL measurements (125°C for 100 s with 50% of the maximum power of the blue LEDs).*

In order to confirm that the measured counts as shown in Fig. 1 and Table 1 were purely from instrumental background, rather than from the possible residual signal of quartz grains, another six blank disks, prepared without mounting any grains, were measured under the same conditions as described above. A mean count rate of 12.7 ± 0.3 cts/0.2 s was obtained, indistinguishable from the value of 13.0 ± 0.1 cts/0.2 s when the grains were present (Table 1). This suggests that no signal came from the annealed quartz grains and there is little dependence of instrumental background on whether the quartz grains were mounted on the disks or not.

The fact that the variance/mean ratio is not 1 for the measurements without grains indicates that the instrumental background doesn't follow a Poisson distribution. Thus the error estimation based on the assumption that the background has a Poisson distribution will lead to underestimation of the true error. It is thus suggested that the instrumental background should be measured for each instrument to check whether it is appropriate to assume a Poisson distribution for the background for error calculation.

The formula for error estimation

Since the background doesn't follow a Poisson distribution, the variances of the slow component and background observed in the final part of an OSL curve need to be considered separately and incorporated into the error calculation for the background-subtracted signal. Using definitions similar to those used by Galbraith (2002), if Y_0 denotes the OSL signal observed in the initial stimulation time (or in the first n channels), by allowing for different OSL components, we have

$$Y_0 = S_{f+m} + S_{s0} + B_0 \qquad \text{Eqn. 1}$$

where S_{f+m} is the fast and medium components in the first n channels, S_{s0} is the slow component and B_0 is the instrumental background in the first n channels. In CW-OSL measurements, S_{f+m} is normally used for dating because it would have been bleached in nature in a short time. However, S_{f+m} cannot be measured directly from the CW-OSL curve. In practice, S_{f+m} is estimated by subtracting an equivalent part at the end of the OSL curve from the initial part (Y_0). This is because the decay rate of the slow component is very slow and can be assumed to be constant during the measurement period (usually 40-100 s). Assuming that S_{f+m}, S_{s0} and B_0 have expectations μ_{f+m} , μ_s and μ_B, and variances σ^2_{f+m}, σ^2_s and σ^2_B respectively, by extending Eqn. 1 in Galbraith's notation (Galbraith, 2002) to allow for the slow component, the variance of the estimate μ_{f+m} is written as

$$Var(\mu_{f+m}) = \sigma^2_{f+m} + \sigma^2_s + \sigma^2_B + \frac{1}{k}\sigma^2_s + \frac{1}{k}\sigma^2_B \qquad \text{Eqn. 2}$$

where k is the ratio of the number (m) of channels used for estimating μ_s and μ_B to the number (n) of channels used for estimating μ_{f+m}.

If S_{f+m}, S_{s0} and B_0 all follow a Poisson distribution, we have $\mu_{f+m} = \sigma^2_{f+m}$, $\mu_s = \sigma^2_s$, and $\mu_B = \sigma^2_B$, and this yields the same expression as equation 3 in Galbraith (2002),

$$RSE(\hat{\mu}_{f+m}) = \frac{\sqrt{Y_0 + \frac{1}{k}\overline{Y}}}{Y_0 - \overline{Y}} \qquad \text{Eqn. 3}$$

where $\overline{Y}$ is the average count per n channels in the last k.n channels, which is an estimate of $\mu_s + \mu_B$. This form is that generally used for error estimation of the background-corrected OSL.

However, if only S_{f+m} and S_{s0} have Poisson distributions, but B_0 does not, thus $\mu_{f+m}=\sigma^2_{f+m}$ and $\mu_s=\sigma^2_s$, but $\mu_B \neq \sigma^2_B$. Then Eqn. 2 becomes

$$Var(\mu_{f+m}) = \mu_{f+m} + (1+\frac{1}{k})\mu_s + (1+\frac{1}{k})\sigma^2_B \qquad \text{Eqn. 4}$$

which can be estimated as

$$Var(\hat{\mu}_{f+m}) = Y_0 - \overline{Y} + (1+\frac{1}{k})(\overline{Y} - \hat{\mu}_B) + (1+\frac{1}{k})\hat{\sigma}^2_B$$

$$= Y_0 + \frac{1}{k}\overline{Y} + (1+\frac{1}{k})(\hat{\sigma}^2_B - \hat{\mu}_B) \qquad \text{Eqn. 5}$$

where $\hat{\sigma}^2_B$ and $\hat{\mu}_B$ are estimates of σ^2_B and μ_B, respectively. Hence the RSE of $\hat{\mu}_{f+m}$ becomes

$$RSE(\hat{\mu}_{f+m}) = \frac{\sqrt{Y_0 + \frac{1}{k}\overline{Y} + (1+\frac{1}{k})(\hat{\sigma}^2_B - \hat{\mu}_B)}}{Y_0 - \overline{Y}} \qquad \text{Eqn. 6}$$

Eqn. 6 is similar to equation 6 given in Galbraith (2002). However, in his note, the source of over-dispersion is not directly known. It has been shown in the section above that the instrumental background is only dependent on the experimental conditions and

instruments, e.g. dark noise of instrument, thickness of filters and power of stimulation light. The values of $\hat{\mu}_B$ and $\hat{\sigma}_B^2$ can thus be obtained by multiplying the average values of the mean counts and variance shown in Table 1 by the channel number n used for obtaining Y_0, providing that the same instrument and measurement conditions are used as those used in measuring annealed quartz with no OSL signal. Hence, the third term $(1+\frac{1}{k})(\hat{\sigma}_B^2 - \hat{\mu}_B^2)$ in the numerator of Eqn. 6, the over-dispersion with respect to the Poisson variation in S_{f+m}, is expected to vary only slightly through all the measurements if the same experimental conditions and instruments are used and can be measured independently.

Dependence of background counts on signal intensity
An important assumption for calculating the background-subtracted OSL signal (as described in the previous section) is that the instrumental background should be independent of the measured signal (i.e. the background contribution of the PMT is the same no matter whether there is the presence of a signal or not). This is difficult/impossible to measure directly, but one possible experiment is to add a constant level of reflected light and look at the residuals around the average level. Such an experiment was carried out by reducing the thickness of the U340 filters from 7.5 mm to 2.5 mm to allow more scattered light to reach the PMT. Four blank discs were then measured four times by holding them at 125°C and using 0%, 10%, 30% and 50% of the maximum power of the blue LED stimulation system, respectively. This would result in different light intensities being measured. The observed mean photon count rate and the corresponding variance for each stimulation power are shown in Fig. 2a and b. As shown, the photon count rate increases linearly with the stimulation power (i.e. scattered light intensity). A similar trend was also observed for the variance, suggesting that the variance of the scattered light also increases with its intensity.

It can be expected that the counts for the scattered light should have a variance/mean ratio independent of its intensity, thus by subtracting the background observed when there is no stimulation light (power=0%) from the total signal with stimulation light (power>0%), the count rate from the scattered light and its variance can be estimated for different stimulation powers. If there is a dependence of background on the measured signal, subtracting the same background from the different signals observed at different stimulation powers would give different calculated variance/mean ratio for the scattered light.

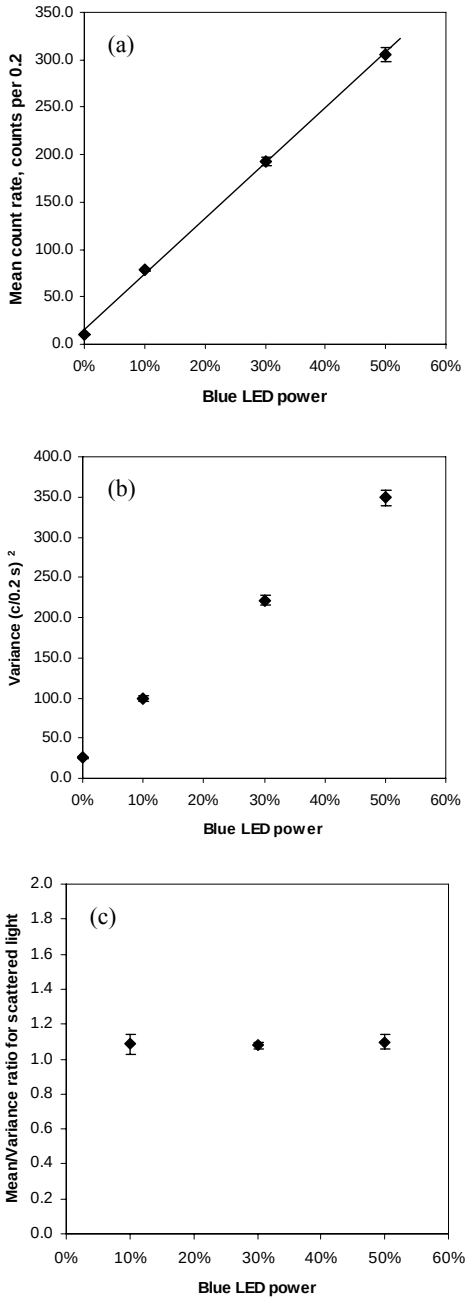

Figure 2: *(a) The observed mean photon count rate plotted against the stimulation light power. (b) The variance for different stimulation powers. (c) The variance/mean ratio of the scattered light obtained by subtracting the background measured when there is no stimulation light.*

On the other hand, if the same variance/mean ratio for the scattered light was obtained by subtracting the same background for different scattered light intensities, it suggests that the background is independent of signal level reaching the PMT. Fig. 2c

Sample	Y_0 (cts/s)	$\bar{Y}$ (cts/s)	RSE (%) Equation 3	RSE (%) Equation 6
C5	209	153	27.5	36.4
Wgs1	775	184	4.8	5.3
TWC	2201	148	2.29	2.35
DGF-1	49061	1273	0.46	0.46

Table 2: *Comparison of the relative standard error (RSE) of the background-corrected OSL signal from four different samples with different levels of OSL signal (see Fig. 3) calculated using Eqn. 3 and 6. Y_0 is the signal counts recorded in the first 1 second (n=5). $\bar{Y}$ is calculated as the average of the signal counts observed in the last 5 seconds (m=25, k=5). The values of $\hat{\mu}_B$ and $\hat{\sigma}_B^2$ are 65 cts/s and 136 (cts/s)^2, repectively, which are estimated by multiplying the mean counts and variance in 0.2 s (Table 1) by the factor k.*

shows the variance/mean ratio of the scattered light plotted as a function of the stimulation power. A similar ratio of ~1.1 was obtained for all stimulation powers used, suggesting that the background is independent of the measured signal. Therefore, one can use the background values obtained by measuring blank discs for calculating the error for the background-subtracted OSL signal as suggested in the previous section.

Effects of the non-Poisson distribution of instrumental background on error estimation

In order to investigate to what extent the nature of the instrumental background may influence the relative standard error (RSE) of the background-corrected OSL signal, typical OSL curves taken from four samples with different levels of OSL counts (Fig. 3) were analyzed using Eqn. 3 and 6, respectively. Y_0 is the signal counts recorded in the first 1 second (n=5).

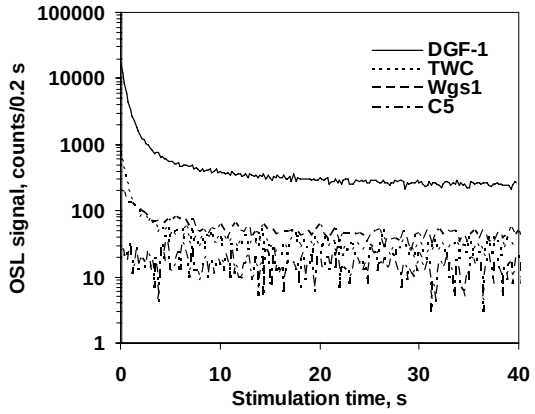

Figure 3: *Typical OSL curves from four samples, C5, Wgs1, TWC and DGF-1, with different levels of OSL count rates. The OSL curves were measured at 125°C using blue LEDs with 50% of the maximum power.*

$\bar{Y}$ is calculated as the average of the signal counts observed in the last 5 seconds (m=25, k=5). The values of $\hat{\mu}_B$ and $\hat{\sigma}_B^2$ are thus 5 times the average values obtained for 0.2 s (Table 1), i.e. $\hat{\mu}_B$=13.0x5=65 and $\hat{\sigma}_B^2$=27.2x5=136 (cts/s)^2 for k=5, respectively.

The value of RSE calculated using different methods are summarized in Table 2. For all samples the RSE values estimated from Eqn. 3 are smaller than those obtained using Eqn. 6. The difference between the RSE obtained from Eqn. 3 and that from Eqn. 6 is reduced as the total OSL counts increase. For the brightest sample DGF-1 (Fig. 3), the two values obtained from the two equations are indistinguishable from each other. This is expected because the contribution from $\hat{\sigma}_B^2$ to the total variance becomes smaller as the OSL signal increases. For the dimmest sample C5 (Fig. 3), the RSE of the background-corrected signal estimated from Eqn. 6 is 38.1%, significantly larger than the value of 27.5% given by Eqn. 3 when assuming that the background has a Poisson distribution.

Discussions

The results suggest that different relative contributions of the slow component and background may result in different counting distributions for the OSL signal and thus different extents of underestimation of the error, if Poisson distribution is simply assumed for all signals, i.e. the OSL signal and instrumental background. Therefore, Eqn. 3 can not be used for estimating the error for weak OSL signals because it may result in significant underestimation of the true error (up to 28% for the dimmest sample C5).

The implication of this result is especially important for young samples and single grains where the signal is relatively weak (e.g. Jain et al., 2004). For these applications, the RSE of the signal is very important for calculating the error in the age and interpreting

the age distribution using radial plots and different age models (e.g. Galbraith, 1990; Galbraith et al., 1999; Jacobs et al., 2006). If the RSE is poorly determined and subsequently used in a radial plot or in age models, e.g. the central age model, this may lead to misinterpretation of the distribution of the age population for the samples. Therefore, Eqn. 6 is recommended for the error estimation of OSL signals, especially those from young samples or dim samples; and this requires the values of $\hat{\mu}_B$ and its variance $\hat{\sigma}_B^2$ to be measured for each instrument. Although the author found that the values of $\hat{\mu}_B$ and $\hat{\sigma}_B^2$ vary negligibly over time, in practice, it is suggested that their values are checked once after every set of OSL measurements. It will be best to use similar discs with completely annealed quartz grains (e.g. annealed at 700°C for one hour) to duplicate the measurement conditions.

Conclusions

The counting distribution of the instrumental background in an OSL measurement is over-dispersed and does not follow a Poisson distribution. This may influence the error estimation of the background-corrected OSL signal substantially, especially for young samples with weak OSL signals.

Acknowledgements

The author thanks Dr. Sheng-hua Li, Prof. Ann Wintle, Prof. Geoff Duller, Dr. Richard Bailey and Prof. Rex Galbraith for their valuable comments.

References

Bailey, R.M., Smith, B.W., Rhodes, E.J., 1997. Partial bleaching and the decay form characteristics of quartz OSL. *Radiation Measurements* **27**, 123-136.

Banerjee, D., Bøtter-Jensen, L., Murray, A.S., 2000. Retrospective dosimetry: estimation of the dose to quartz using the single-aliquot regenerative-dose protocol. *Applied Radiation and Isotopes* **52**, 831-844.

Bøtter-Jensen, L., Duller, G.A.T., Murray, A.S., Banerjee, D., 1999. Blue light emitting diodes for optical stimulation of quartz in retrospective dosimetry and dating. *Radiation Protection Dosimetry* **84**, 335-340.

Galbraith, R.F., 1990. The radial plot: graphical assessment of spread in ages. *Nuclear Tracks and Radiation Measurements* **17**, 207-214.

Galbraith, R.F., 2002. A note on the variance of a background corrected OSL count. *Ancient TL* **20**, 49–51.

Galbraith, R.F., Roberts, R.G., Laslett, G.M., Yoshida H., Olley, J.M., 1999. Optical dating of single and multiple grains of quartz from Jinmium rock shelter, northern Australia: Part I, Experimental design and statistical models. *Archaeometry* **41**, 339–364.

Jacobs, Z., Duller, G.A.T., Wintle, A.G., 2006. Interpretation of single grain D_e distributions and calculation of D_e. *Radiation Measurements* **41**, 264-277.

Jain, M., Thomsen, K. J., Bøtter-Jensen, L., Murray, A. S., 2004. Thermal transfer and apparent-dose distributions in poorly bleached mortar samples: results from single grains and small aliquots of quartz. *Radiation Measurements* **38**, 101-109.

Li, B., Li, S.H., 2006. Comparison of D_e estimation using the fast component and the medium component of the quartz OSL. *Radiation Measurements* **41**, 125-136.

Smith, B.W., Rhodes, E.J., 1994. Charge movements in quartz and their relevance to optical dating. *Radiation Measurements* **23**, 329-333.

Reviewer

R.M. Bailey

Assessing the error on equivalent dose estimates derived from single aliquot regenerative dose measurements

G.A.T. Duller

Institute of Geography and Earth Sciences, University of Wales Aberystwyth, Ceredigion SY23 3DB, United Kingdom

(Received 3 May 2007; in final form 6 June 2007)

Introduction

Measurement of the equivalent dose (D_e) is central to luminescence dating. Single aliquot methods have been developed in the last 10-15 years, first with the description of methods suitable for feldspars (Duller 1995) and subsequently those applicable to quartz (Murray and Wintle 2000, 2003). Such methods have the advantage that they are comparatively rapid, making it feasible to generate replicate determinations of the D_e, and generally yield D_e values of greater precision than multiple aliquot methods (e.g. Hilgers et al. 2001).

The ability to make replicate measurements of the D_e is one of the most significant advantages of single aliquot methods since this makes it possible to explicitly assess the distribution of apparent dose. This may be critical to demonstrate whether a sample was well bleached at deposition, and whether it has suffered from post-depositional mixing (e.g. Roberts et al. 1998; Jacobs et al. 2003). A number of approaches have been suggested for both displaying and analyzing dose distributions (Galbraith et al. 1999; Thomsen et al. 2003; Spencer et al 2003; Galbraith 2003), but implicit to all these approaches is the assumption that the uncertainty in the individual D_e values is known.

Variations in D_e between different grains can be masked if many grains are measured simultaneously in a single aliquot (Wallinga 2002), and thus most analyses designed to study the dose distribution are undertaken on aliquots containing few grains (typically 20-50) or single grains. At this scale of analysis, not only do any variations in D_e become apparent, but so too do variations in the brightness of individual grains (McFee and Tite 1998; Duller et al. 2000; McCoy et al. 2000). One effect of such variations in brightness is that the precision with which D_e can be calculated varies from one aliquot to another. As shown by Bailey and Arnold (2006), accurately assessing the error on the D_e is vital in these situations if any method is used to combine these results that relies upon weighting the results depending upon the accuracy of the individual results (e.g. the Central Age model or Minimum Age model, Galbraith et al. 1999).

Sources of uncertainty in the D_e can be subdivided into random and systematic sources. This paper only deals with random errors associated with the luminescence measurements and then their combination to determine D_e. Systematic sources of uncertainty, such as errors in the calibration of the beta or gamma source used to irradiate the sample in the laboratory need to be considered after the combination of individual D_e values. Similarly, there is an additional source of uncertainty in the suitability of the material for use with the SAR procedure; such uncertainty will be material dependent and has been the subject of much discussion by many authors (e.g. Bailey 2000; Murray et al. 2002; Jacobs et al. 2006a). Such issues are likely to become more significant as the luminescence signal gets close to saturation. The aim of this paper is to compare various approaches to estimating the error on individual D_e values, and provide some data sets that other workers may wish to analyse using their own methods. The paper will focus on examples where the growth is linear, or approximately linear.

Methods of D_e determination

The process of calculating D_e using the SAR procedure involves measurement of the natural luminescence signal (L_N) arising from irradiation in nature, assessing the sensitivity of the aliquot by measuring the luminescence signal (T_N) generated by a test dose (D_T), and then undertaking a number of cycles each of which involves irradiation (D_1, D_2, D_3 etc) to regenerate the luminescence signal (L_1, L_2, L_3 etc), followed by a test of the sensitivity (T_1, T_2, T_3 etc) using the test dose. The value of D_e is then found by comparing the ratio R_N (= L_N/T_N) with the ratios R_1, R_2, R_3 etc (obtained from L_1/T_1, L_2/T_2, L_3/T_3 etc) to determine the laboratory dose that generates a signal equivalent to that obtained from the natural.

While all methods for determining D_e are very similar, for the purpose of this paper they can be grouped into three main categories. The simplest method is to compare the normalised signal from the natural ($R_N = L_N/T_N$) with that from the regeneration measurement which gives the closest ratio (e.g. $R_1 = L_1/T_1$) (Fig. 1a). The D_e is then simply given by the ratios of the signals and the dose (D_1) given in the laboratory to generate R_1:

$$D_e = \frac{R_N}{R_1} D_1 \qquad \text{Eqn. 1}$$

The second method is to interpolate between two regeneration points (R_1 and R_2), one of which is larger than R_N, and one of which is smaller (Fig. 1b). As with the first method, the mathematical calculation of the D_e is straightforward, and relies upon the three ratios of the luminescence signals, and the two known laboratory doses D_1 and D_2 given to the aliquot to generate R_1 and R_2:

$$D_e = \frac{(R_N - R_1)}{(R_2 - R_1)}(D_2 - D_1) + D_1 \qquad \text{Eqn. 2}$$

The third method is to measure the response of the aliquot to a number of different regeneration doses (D_1, D_2, D_3 etc), and to fit an appropriate mathematical equation to the resulting data set R_1, R_2, R_3 etc (Fig. 1c). The equation fitted to this growth curve may be a straight line, or more commonly something involving a saturating exponential (e.g. Eqn. 3), reflecting the commonly accepted view that the luminescence signal saturates at high doses as the defect sites within the aliquot being measured become full.

$$R(D) = I_{Max}(1 - e^{-\frac{D}{D_0}}) + c \qquad \text{Eqn. 3}$$

The ratio R(D) (e.g. R_1, R_2, R_3 etc) measured following a laboratory dose, D, is dependent on the characteristic dose D_0, which characterises the rate at which the defects in the aliquot become full, the maximum value obtainable, I_{Max}, and an offset, c. For the results shown in this paper the Levenberg-Marquardt algorithm has been used to fit both linear and saturating exponential functions. Hayes et al. (1998) have previously shown that such an algorithm can be used successfully for luminescence data, and the numerical routine from Press et al. (1986) is a convenient source of code.

Each of these methods have implicit assumptions regarding the form of the dose response. For the first method it is assumed that the dose response (R_i) is proportional to dose (D_i) over the interval being analysed; for the second method that the dose response is linear between R_1 and R_2; and for the third method, that the chosen function adequately describes the dose response form. If these

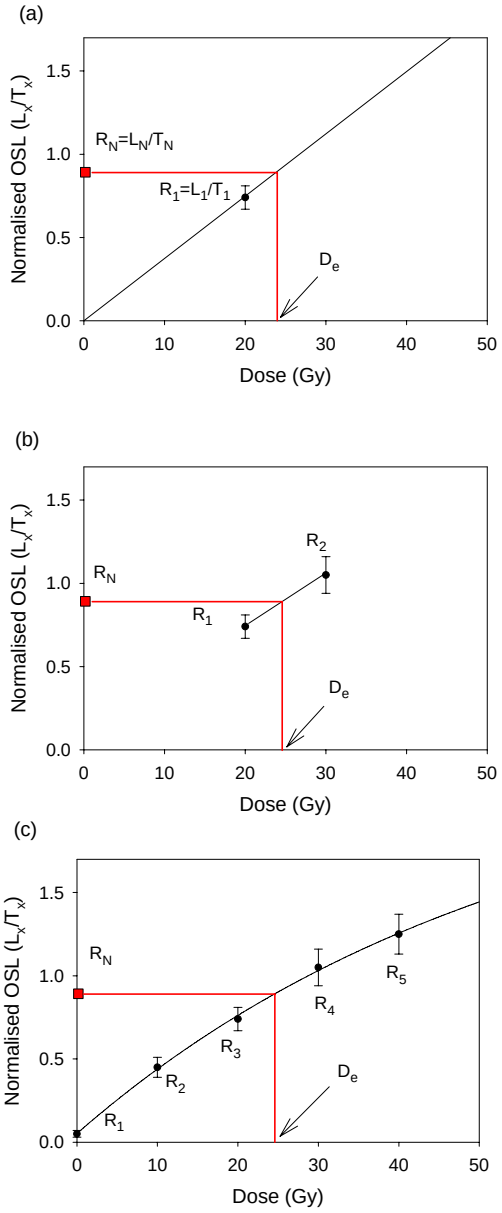

Figure 1: *Diagram illustrating the three means of using SAR data to obtain a value of D_e. (a) By taking the ratio of R_N and a single value of R_X, (b) by interpolating between two values of R_X that straddle R_N, and (c) fitting a number of values of R_X measured at different regeneration doses to an equation (e.g. saturating exponential), and then interpolating the value of R_N onto that curve to determine D_e.*

Instrumental Error (%)	L_{Signal}	L_{BG}	T_{Signal}	T_{BG}	R_x	S_{Rx}	$\frac{S_{Rx}}{R_x} \times 100$
0	1,050	50	550	50	2.000	0.118	5.9%
1	1,050	50	550	50	2.000	0.122	6.1%
0	100,050	50	50,050	50	2.000	0.011	0.6%
1	100,050	50	50,050	50	2.000	0.030	1.5%

Table 1: *Examples of the uncertainty (S_{RX}) in the ratio of L_X/T_X (=R_X) from counting statistics and from instrumental error.*

assumptions are not met then this will introduce error into the value of D_e obtained, but such errors are unlikely to be estimated correctly by the methods described in this paper.

Sources of uncertainty in D_e

Assessing the error in the final value of D_e determined using these methods can be divided into two stages. The first involves calculating the uncertainty in each luminescence measurement and hence the ratios L_x/T_x, whether that is the ratio for the natural or a regeneration dose. The second stage is transforming the errors in those ratios, into an estimate of the uncertainty in the dose, D_e.

Errors in individual L/T ratios

The first constraint on the ability to measure a luminescence signal is its intensity. The uncertainty due to the counting statistics can be calculated using the method described in Galbraith (2002) based on a combination of both the number of counts in the signal and the magnitude of the background signal (L_{BG}) that has been subtracted. Li (2007) has shown that the situation becomes more complex at very low signal levels, but for this paper the approach of Galbraith (2002) has been used. The errors on the values of L_X and T_X can then be propagated in quadrature through Eqn. 4 to give the standard deviation S_{Rx}.

$$S_{R_x} = S_{\frac{L_x}{T_x}} = \frac{L_x}{T_x}\sqrt{\left[\frac{L_{Signal}+L_{BG}}{\left(L_{Signal}-L_{BG}\right)^2}\right]+\left[\frac{T_{Signal}+L_{BG}}{\left(T_{Signal}-L_{BG}\right)^2}\right]}$$

Eqn. 4

A second source of uncertainty arises from the equipment used to undertake the irradiation, heating and optical stimulation of the aliquot. This uncertainty may be due to small variations in the intensity of the optical stimulation source, small variations in aliquot positioning under the radiation source or under the optical stimulation source, and small variations in the temperature of the aliquot both during preheating and during measurement. The magnitude of these effects is difficult to quantify individually, but collectively they may be termed 'instrumental error'. These effects are likely to be small, but for bright samples where the uncertainty due to counting statistics is small, they may make a significant contribution to the total uncertainty. The size of this instrumental error can be assessed by making repeated measurements of the luminescence signal from a given irradiation. Such measurements have been undertaken for a standard Risø TL/OSL system by Armitage et al. (2000) giving an instrumental error of 1% on each measurement of L and T. A similar measurement by Rodnight (2006, p.167) yielded a larger value of 2.5%. Thomsen et al. (2005) and Jacobs et al. (2006b) made similar measurements for a single grain system, giving instrumental errors of ~1.5%. It is likely that this value may vary from one instrument to another, and possibly may change over long periods of time as instruments alter in their operation. For this paper a value of 1% has been used, and this contribution needs to be combined in quadrature with that from counting statistics for each L_X/T_X ratio.

A feeling for the magnitude of these effects, and their relative importance, can be gained from taking a number of examples. Table 1 shows data for a single aliquot measurement which gives a signal (L_{Signal}) of 1050 counts, a background (L_{BG}) of 50 counts, a test dose response (T_{Signal}) of 550 counts and a background (T_{BG}) of 50 counts, giving a ratio of L_x/T_x of 2.000. Based solely on the counting statistics, and using Eqn. 4, the standard deviation in that ratio is 0.118 (5.9%). Including the value of 1% for the instrumental error only marginally increases this to 6.1%, and the dominant source of uncertainty is the low count rate. In the second example in Table 1, the aliquot is approximately one hundred times brighter, and so the uncertainty due to counting statistics is very low (0.6%). In this case the instrumental error more than doubles this (1.5%).

Transforming the error in L/T ratios to an error in D_e

The quantity that we are ultimately interested in is the D_e and the standard deviation of this value (S_{De}). The approach to estimating S_{De} varies depending upon the method used to determine D_e. Using Eqn. 1, the

uncertainty can be simply obtained by combining the errors in the two ratios R_N and R_1 in quadrature, giving the following equation:

$$S_{D_e} = D_e \sqrt{\left(\frac{S_{R_N}}{R_N}\right)^2 + \left(\frac{S_{R_1}}{R_1}\right)^2} \qquad \text{Eqn. 5}$$

For the situation where one is interpolating between two data points, as expressed in Eqn. 2, Thomsen et al. (2005, 2007) have shown that the standard deviation in the value of D_e is given by the expression in Eqn. 6.

$$S_{D_e} = \sqrt{\left(\frac{D_2 - D_1}{R_2 - R_1}\right)^2 \left\{ S_{R_N}^2 + \left(\frac{1}{R_2 - R_1}\right)^2 \left[(R_N - R_2)^2 S_{R_1}^2 + (R_N - R_1)^2 S_{R_2}^2 \right] \right\}}$$

Eqn. 6

In the more complex situation where a large number of values of R_x are used to fit a mathematical equation to define the growth of the luminescence signal, then defining an analytical solution for the standard deviation in the D_e becomes more complex. For simple functions (e.g. linear) then it may be possible to do this, but in such methods it is normally necessary that the errors are relatively small. This is not always the case in luminescence data. The question then arises of how one can assess the value of S_{De}?

Simple transformation of the S_{RN} to S_{De}

Frequently for luminescence data obtained using the SAR procedure, one of the dominant sources of uncertainty arises from measurement of the natural (S_{RN}) due to counting statistics and instrumental error. A straightforward means to estimate the uncertainty in the D_e that results from this is to interpolate the values $R_N + S_{RN}$ and $R_N - S_{RN}$ onto the growth curve and then see the variation in D_e that results. This approach makes it possible to deal with any form of equation that is fitted to the growth curve, and accommodates changes in curvature of the growth curve. However, it does not take into account the degree of certainty with which the growth curve is known, based upon the fit to the data R_1, R_2, R_3 etc. A first order approximation to incorporate the uncertainty in the growth curve that has been fitted can be obtained by calculating the deviation of the fitted growth curve from the n data points $R_{1..n}$ using Eqn. 7.

$$Average\ Deviation = \sqrt{\frac{\sum_{i=1}^{i=n} (Predicted\ R_i - Actual\ R_i)^2}{n}} \qquad \text{Eqn. 7}$$

This figure for the typical deviation of the fitted growth curve from the measured data points is then combined in quadrature with the uncertainty in the ratio of R_N. This combined error is then transformed through interpolation of the upper and lower limits of R_N on to the growth curve, to calculate the limits on the estimate of D_e. Such an approach has the advantage of speed, but how accurate is such an approximation, and is a better approach available?

The Monte Carlo method

A more robust approach to assessing the error on the value of D_e is to use a Monte Carlo method (Press et al. 1986). This approach has been used by some researchers for a number of years (Bailey Pers. Comm., e.g. Grine et al. 2007). Each value of R_x and its standard deviation S_{RX}, based on counting statistics and instrumental error, is represented by a Gaussian distribution of possible values. Repeated curve fitting and calculation of D_e are undertaken where the values of R_x that are used both for R_N, and for R_1, R_2, R_3 etc are drawn from Gaussian distributions whose widths are set by the calculated standard deviations. This approach explicitly assesses the nature of the distribution in the value of D_e, including its width and whether it is symmetric. An estimate of the standard deviation of D_e can then be explicitly calculated by analysis of the resulting distribution of D_e values. The central value of D_e is still obtained using the best fit through the original data.

Example data sets

To provide a comparison of these different approaches, a number of example data sets are shown (Fig. 2), and the results of D_e determination using the different methods and appropriate error calculations are shown in Table 2. The luminescence data used to generate the graphs in Fig. 2 are given in the Appendix. Although this is a limited data set with which to compare the methods, a number of points can be made.

Firstly, given the data sets used here, the results are consistent between the different methods. Given the variety of approaches both to determining the D_e and its uncertainty, this is reassuring. Moreover, the approximation described in the section headed "*Simple transformation of the S_{RN} to S_{De}*" (shown under the heading "Curve Fitting" in Table 2) gives uncertainties that are very close to those derived using the more complex Monte Carlo approach. The Monte Carlo method is more time consuming than the approximation. The uncertainties shown in the final column of Table 2 are based on 1000 estimates of D_e using the Monte Carlo method (the distribution of D_e values are shown as histograms below the

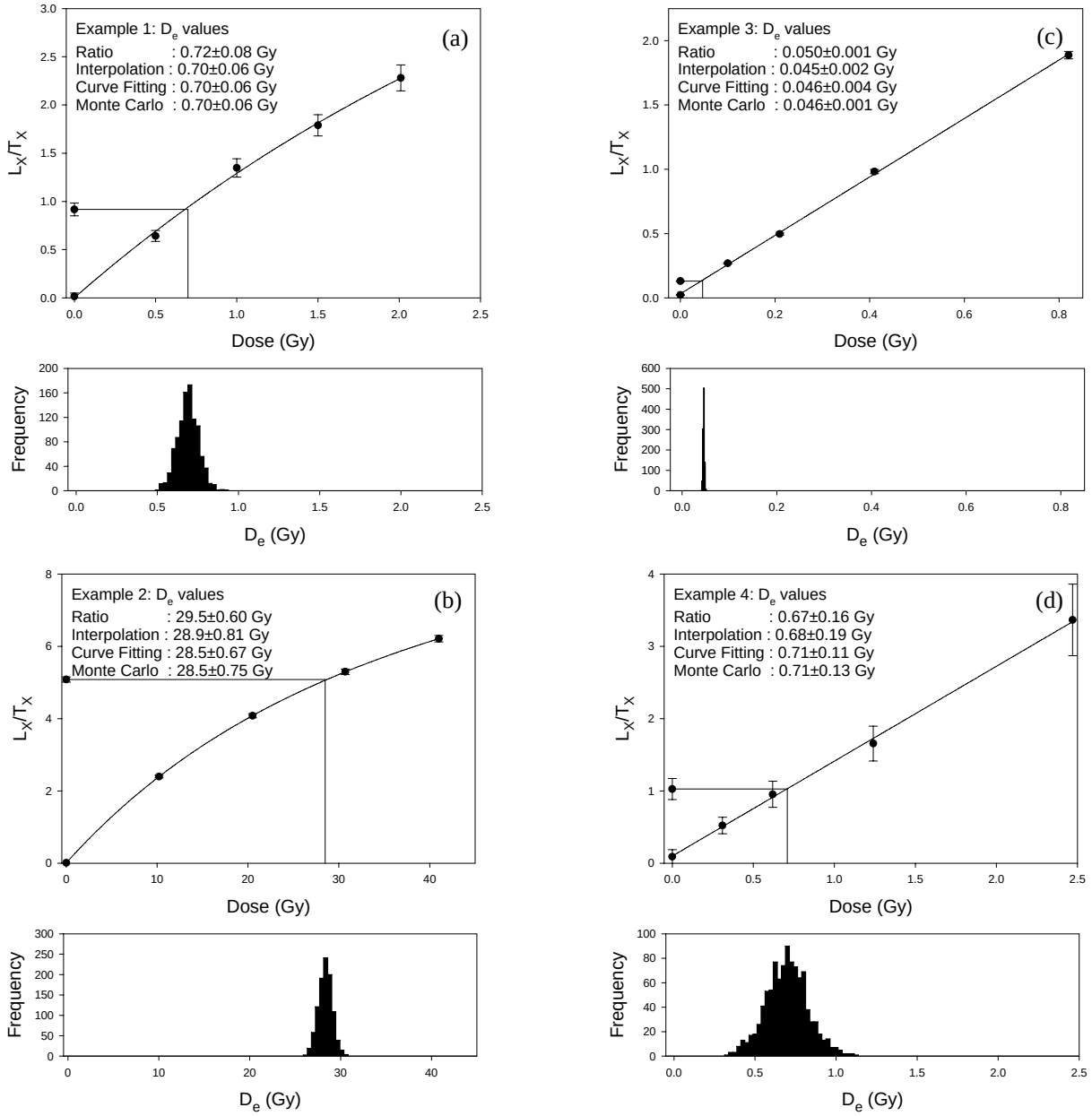

Figure 2: *Growth curves for four example SAR data sets. In each case the values of L_X/T_X have been calculated based on the counting statistics and incorporating a 1% instrumental error. The D_e value indicated on each diagram is that based on curve fitting. The distribution of D_e values obtained using 1000 iterations of the Monte Carlo method are shown in the figures below each growth curve.*

Example Number	Equivalent Dose (Gy)				
	Ratio	Interpolate	Equation fitted	Curve Fitting	Monte Carlo
1	0.72±0.08	0.70±0.06	Exponential	0.70±0.06	0.70±0.06
2	29.5±0.60	28.9±0.81	Exponential	28.5±0.67	28.5±0.75
3	0.050±0.001	0.045±0.002	Linear	0.046±0.004	0.046±0.001
4	0.67±0.16	0.68±0.19	Linear	0.71±0.11	0.71±0.13

Table 2: *Comparison of equivalent dose calculated using the different analytical procedures described in the text.*

growth curves in Fig. 2). However, the greater statistical robustness of the Monte Carlo method for determining the errors makes it preferable.

In general, measuring R_X for a range of regeneration doses provides information about the form of the growth of the luminescence signal. This is particularly important where the natural luminescence signal R_N may be close to saturation. Using a single data point and calculating the D_e by the ratio of R_N to R_X should provide an accurate value, especially where the D_e is low. However, the D_e may be inaccurate if the value of R_X does not closely match R_N. In the data sets shown in Fig. 2, this is not a major problem since R_X values at a range of doses have been measured, and the value of D_e shown in Table 2 is calculated by taking the ratio of R_N to R_X for that value of R_X that is closest to R_N. In spite of this, it can be observed that the D_e for Example 2 determined by this method (29.5±0.60 Gy) is higher than that calculated using the other methods, because the value of R_X used (that relating to a regeneration dose of 30.7 Gy) is higher than R_N, and the method implicitly assumes that the growth of R_X is linear with dose. Using the value of R_X from the 41.0 Gy regeneration point gives an even higher D_e of 33.5±0.68 Gy. Conversely, using values of R_X below R_N gives lower D_e values. Had the regeneration point at 20.5 Gy been used then the D_e would be 25.5±0.52 Gy, and using the 10.2 Gy regeneration data would yield a D_e of 21.7±0.44 Gy.

Interpolating between the two values of R_X that straddle R_N overcomes this fundamental problem, and approximates the slope of the growth curve at that dose. However, once again, the closer the two values of R_X are to R_N, the better the estimate of D_e. Precisely matching R_X and R_N is often difficult because of variability in the D_e from one aliquot to another. The best estimate of the form of the growth curve near R_N is achieved by fitting an equation to the entire data set.

Dose recovery experiment

One means of assessing whether the estimation of the errors on D_e values is appropriate is to undertake a dose recovery experiment on a sample that is thought to be well suited for the SAR procedure. Quartz extracted from a linear dune in north-eastern Tasmania (TNE9517, Duller and Augustinus 2006) was used for this experiment. Quartz grains were 180-211 μm in diameter, and these were mounted on aluminium discs using silicone oil. In order to create data with different OSL signal intensities, and thus with different uncertainties due to counting statistics, 22 aliquots were prepared so that the grains covered an area of ~5 mm diameter, while another 16 aliquots were prepared where the grains covered an area of 2 mm diameter.

The OSL properties of quartz from this part of Tasmania have been described briefly in Duller and Augustinus (2006). The quartz has an intense OSL signal, and yields reproducible values of D_e using the SAR procedure. To undertake the dose recovery experiment, the 38 aliquots were bleached using the blue diodes in a Risø TL/DA-15 TL/OSL reader, given a dose of ~5 Gy using the $^{90}Sr/^{90}Y$ beta source mounted on the reader, preheated at 220°C for 10 seconds, and then had their OSL signal measured while holding them at 125°C. The aim of this test was not to assess the extent to which the sample is suitable for the SAR procedure, but to assess whether the calculation of the error in the calculation of D_e is appropriate. Thus, the bleaching and irradiation procedure was repeated at least 4 times in an attempt to 'condition' the aliquots and make them as reproducible as possible.

For the experiment itself, the 38 aliquots were exposed to the beta source for 15 seconds (~ 0.6 Gy). The magnitude of this dose was then determined using a SAR procedure, with 6 regeneration doses (0, 10, 20, 30, 40, 10 seconds beta dose), using a preheat of 220°C for 10 seconds, and a cutheat after the test dose (6 seconds beta dose) of 200°C. After measurement of the response to the test dose, the aliquots were exposed to the blue diodes for 40 s whilst holding them at 280°C in order to reduce any build up of slow components in the OSL signal (Murray and Wintle 2003).

The equivalent dose values and associated errors were calculated using the Curve Fitting method and the Monte Carlo method. Both sets of analysis were undertaken assuming an instrumental uncertainty of 1.0%, and the results are shown as radial plots in Fig. 3. There is a broad spread in the precision with which the values are known, as was hoped for by the use of two different aliquot sizes. In both analyses, the results are consistent with the given dose of 15 s (weighted mean is 14.6±0.7 and 14.7±0.7 s respectively for the two analyses). In detail the errors on the D_e values are subtly different. For the Curve Fitting method, 35 out of 38 of the aliquots (92%) are consistent with 15 s within two standard deviations, while for the Monte Carlo method 33 out of 38 (87%) are consistent. Both percentages are only slightly lower than would be expected from statistics (for a normal distribution, 95% of the data are within two standard deviations).

It is interesting to note that while the two radial plots are similar, there are differences. For instance the

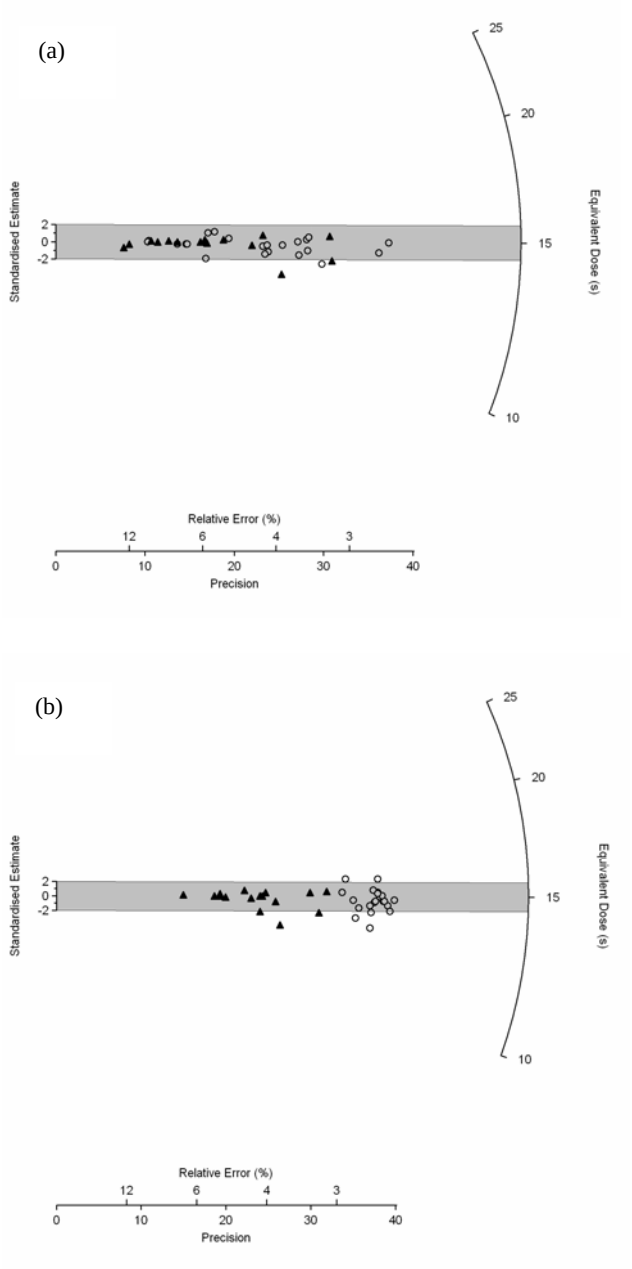

Figure 3: *Radial plot of 38 D_e values obtained in a dose recovery experiment. The aliquots were irradiated for 15 s (~0.6 Gy), and then an SAR growth curve was constructed to measure this dose. The data were analysed (a) using the Curve Fitting procedure and (b) using the Monte Carlo method. Open points are those obtained using 5 mm diameter aliquots, filled points are those for 2 mm aliquots.*

range in Relative Error observed is 2.7-13.1% for the Curve Fitting method, but rather narrower for the Monte Carlo method (2.5-6.7%). For a single population such as that shown in Fig. 3 this difference is unimportant, but it may have a more serious impact if a data set containing a wide distribution of D_e values were to be analysed using some form of statistical model such as the Minimum Age model (Galbraith et al. 1999). Assessing the sensitivity of such statistical procedures to changes in the calculated uncertainty in D_e has been assessed by Bailey and Arnold (2006), who shows the importance of reliably estimating it.

Conclusions

While there are differences between the D_e values obtained using the three methods of D_e determination illustrated in Fig. 1, these differences are small (Table 2). For these data sets, R_X has been measured for a range of different regeneration doses to ensure that the response of the luminescence signal in the dose range of interest is known. Using the ratio to a single data point may lead to larger errors than those seen here if the value of R_X is not close to R_N, or if the aliquot is close to saturation. Interpolating between two values of R_X decreases the magnitude of any such error, but the most accurate method will be to fit the entire data set, particularly if there is discernable deviation from linear growth. Two methods of estimating the standard deviation in the estimate of D_e have been described. Of the two, the Monte Carlo approach is more statistically robust, but both yield similar results, both for the detailed examples shown in Fig. 2, and the dose recovery data in Fig. 3, presumably because the dominant source of uncertainty is that which arises from the measurement of R_N and the instrumental error. One advantage of the Monte Carlo approach is that for samples approaching saturation it will correctly identify that the errors in the estimate of D_e are asymmetric. However, two issues arise in such situations. The first is that standard statistical methods for combining different D_e estimates which rely upon weighting of individual data points cannot easily be applied to data with asymmetric errors. The second is that in situations where the luminescence growth curve is sufficiently close to saturation for asymmetry in errors to become important, the reliability of the SAR method is unclear. Wintle and Murray (2006) recommend that the method only be used when R_N is less than 85% of I_{Max} (Eqn. 3).

While the procedures described here attempt to assess the random uncertainty in the estimates of D_e obtained using the SAR procedure, the error due to systemic failures of the SAR procedure, or inappropriate response of the dosemeter will not be captured. These could potentially be very large, and are likely to become more severe as the response of the aliquot to radiation decreases as it approaches saturation. Such effects are more difficult to assess,

and tests such as dose recovery experiments may be one of the few ways that it is possible to get some impression of their impact.

Acknowledgements

All analyses shown here, including the Monte Carlo calculations, have been performed using the software package Analyst (Version 3.24) which is now available. The author is very grateful to a large number of people who have provided encouragement and help in the development of this software over many years. Kristina Thomsen very kindly provided the opportunity to test a number of these routines and gave assistance in checking some of the calculations. Richard Bailey discussed Monte Carlo methods and provided extremely helpful suggestions that improved this paper. Ann Wintle and Helen Roberts also provided valuable comments on earlier versions of the paper.

References

Armitage, S. J., Duller, G. A. T., Wintle, A. G. (2000). Quartz from southern Africa: sensitivity changes as a result of thermal pretreatment. *Radiation Measurements* **32**, 571-577.

Bailey, R. M. (2000). Circumventing possible inaccuracies of the single aliquot regeneration method for the optical dating of quartz. *Radiation Measurements* **32**, 833-840.

Bailey, R. M., Arnold, L. J. (2006). Statistical modelling of single grain quartz D_e distributions and an assessment of procedures for estimating burial dose. *Quaternary Science Reviews* **25**, 2475-2502.

Duller, G. A. T. (1995). Luminescence dating using single aliquots: methods and applications. *Radiation Measurements* **24**, 217-226.

Duller, G. A. T., Bøtter-Jensen, L., Murray, A. S. (2000). Optical dating of single sand-sized grains of quartz: sources of variability. *Radiation Measurements* **32**, 453-457.

Duller, G. A. T., Augustinus, P. C. (2006). Reassessment of the record of linear dune activity in Tasmania using optical dating. *Quaternary Science Reviews* **25**, 2608-2618.

Galbraith, R. F. (2002) A note on the variance of a background-corrected OSL count. *Ancient TL* 20, 49-51.

Galbraith, R. F. (2003). A simple homogeneity test for estimates of dose obtained using OSL. *Ancient TL* **21**, 75-77.

Galbraith, R. F., Roberts, R. G., Laslett, G. M., Yoshida, H., Olley, J. M. (1999). Optical dating of single and multiple grains of quartz from Jinmium rock shelter, northern Australia: Part I, Experimental design and statistical models. *Archaeometry* **41**, 339-364.

Grine, F. E., Bailey, R. M., Harvati, K., Nathan, R. P., Morris, A. G., Henderson, G. M., Ribot, I., Pike, A. W. G. (2007). Late Pleistocene human skull from Hofmeyr, South Africa, and modern human origins. *Science* **315**, 226-229.

Hayes, R. B., Haskell, E. H., Kenner, G. H. (1998) An assessment of the Levenberg-Marquardt fitting algorithm on saturating exponential data sets. *Ancient TL* 16, 57-62.

Hilgers, A., Murray, A. S., Schlaak, N., Radtke, U. (2001). Comparison of quartz OSL protocols using lateglacial and Holocene dune sands from Brandenburg, Germany. *Quaternary Science Reviews* **20**, 731-736.

Jacobs, Z., Duller, G. A. T., Wintle, A. G. (2003). Optical dating of dune sand from Blombos Cave, South Africa: II - single grain data. *Journal of Human Evolution* **44**, 613-625.

Jacobs, Z., Duller, G. A. T., Wintle, A. G. (2006b). Interpretation of single grain D_e distributions and calculation of D_e. *Radiation Measurements* **41**, 264-277.

Jacobs, Z., Wintle, A. G., Duller, G. A. T. (2006a). Evaluation of SAR procedures for D_e determination using single aliquots of quartz from two archaeological sites in South Africa. *Radiation Measurements* **41**, 520-533.

Li, B. (2007). A note on estimating the error when subtracting background counts from weak OSL signals. *Ancient TL* **25**, 9-14.

McCoy, D. G., Prescott, J. R., Nation, R. J. (2000). Some aspects of single-grain luminescence dating. *Radiation Measurements* **32**, 859-864.

McFee, C. J., Tite, M. S. (1998). Luminescence dating of sediments - the detection of high equivalent dose grains using an imaging photon detector. *Archaeometry* **40**, 153-168.

Murray, A. S., Wintle, A. G. (2000). Luminescence dating of quartz using an improved single-aliquot regenerative-dose protocol. *Radiation Measurements* **32**, 57-73.

Murray, A. S., Wintle, A. G. (2003). The single aliquot regenerative dose protocol: potential for improvements in reliability. *Radiation Measurements* **37**, 377-381.

Murray, A. S., Wintle, A. G., Wallinga, J. (2002). Dose estimation using quartz OSL in the non-linear region of the growth curve. *Radiation Protection Dosimetry* **101**, 371-374.

Press, W. H., Flannery, B. P., Teukolsky, S. A., Vetterling, W. T. (1986). *Numerical Recipes: The art of scientific computing*. Cambridge University Press.

Roberts, R. G., Bird, M., Olley, J., Galbraith, R., Lawson, E., Laslett, G., Yoshida, H., Jones, R., Fullagar, R., Jacobsen, G., Hua, Q. (1998). Optical and radiocarbon dating at Jinmium rock shelter in northern Australia. *Nature* **393**, 358-362.

Rodnight H. (2006). *Developing a luminescence chronology for Late Quaternary fluvial change in South African floodplain wetlands.* Unpublished PhD thesis, University of Wales Aberystwyth, 304pp.

Spencer, J. Q., Sanderson, D. C. W., Deckers, K., Sommerville, A. A. (2003). Assessing mixed dose distributions in young sediments identified using small aliquots and a simple two-step SAR procedure: the F-statistic as a diagnostic tool. *Radiation Measurements* **37**, 425-431.

Thomsen, K. J., Jain, M., Bøtter-Jensen, L., Murray, A. S., Jungner, H. (2003). Variation with depth of dose distributions in single grains of quartz extracted from an irradiated concrete block. *Radiation Measurements* **37**, 315-321.

Thomsen, K. J., Murray, A. S., Bøtter-Jensen, L. (2005). Sources of variability in OSL dose measurements using single grains of quartz. *Radiation Measurements* **39**, 47-61.

Thomsen, K.J., Murray A.S., Bøtter-Jensen L., Kinahan J. (2007) Determination of burial dose in incompletely bleached fluvial samples using single grains of quartz. *Radiation Measurements* **42**, 370-379

Wallinga, J. (2002). On the detection of OSL age overestimation using single-aliquot techniques. *Geochronometria* **21**, 17-26.

Wintle, A. G., Murray, A. S. (2006). A review of quartz optically stimulated luminescence characteristics and their relevance in single-aliquot regeneration dating protocols. *Radiation Measurements* **41**, 369-391.

Appendix:

The luminescence data used to construct the growth curves in Fig. 2 are shown in the tables overleaf. In each case an instrumental error of 1% was used in the calculations. The luminescence signals were integrated from channels 1-10, and the background from channels 231-250. In the tables below, the value of the background has been adjusted to allow for the difference in the number of channels used for integration.

Reviewer

R.M. Bailey

Example 1

	L_x		T_x			
Dose (Gy)	Signal	BG	Signal	BG	L_x/T_x	$S(L_x/T_x)$
Natural	967	270	1064	304	0.917	0.066
2.01	2157	316	1219	412	2.281	0.134
1.50	1748	361	1139	364	1.790	0.110
1.00	1338	367	1122	401	1.347	0.095
0.50	870	364	1163	375	0.642	0.056
0.00	372	360	1159	383	0.015	0.035

Example 2

	L_x		T_x			
Dose (Gy)	Signal	BG	Signal	BG	L_x/T_x	$S(L_x/T_x)$
Natural	1961354	8978	398551	14323	5.081	0.072
0.0	13317	9690	353432	14664	0.011	0.000
10.2	680491	21238	294425	19112	2.395	0.034
20.5	983391	28554	256435	22292	4.078	0.059
30.7	1202981	36036	246823	26456	5.295	0.076
41.0	1445211	45549	257434	32002	6.209	0.089

Example 3

	L_x		T_x			
Dose (Gy)	Signal	BG	Signal	BG	L_x/T_x	$S(L_x/T_x)$
Natural	6566	968	44775	1798	0.130	0.003
0.82	83842	2268	46127	2918	1.888	0.029
0.41	44984	2683	46302	3234	0.982	0.016
0.21	24094	2682	46589	3390	0.496	0.008
0.10	14088	2788	45560	3486	0.269	0.005
0.00	3626	2676	46666	3458	0.022	0.002

Example 4

	L_x		T_x			
Dose (Gy)	Signal	BG	Signal	BG	L_x/T_x	$S(L_x/T_x)$
Natural	294	93	294	98	1.026	0.145
0.00	120	106	281	126	0.090	0.098
0.31	221	122	318	128	0.521	0.114
0.62	313	151	342	172	0.953	0.180
1.24	536	200	402	199	1.655	0.242
2.47	934	268	466	268	3.364	0.495

Temperature calibration and MiniSys temperature upgrade for the Risø TL/OSL-DA-15 reader

K.J. Thomsen

Radiation Research Department, Risø National Laboratory, Technical University of Denmark, DK 4000 Roskilde, Denmark

(Received 27 April 2007; in final form 3 May 2007)

Introduction

In both TL and OSL measurements it is important to have accurate control over the thermal treatment of samples. In the Risø TL/OSL reader heating is performed using a low-mass heater strip made of Kanthal (a high resistance alloy) which is shaped with a depression to provide a better contact with the planchet or disc (Bøtter-Jensen 1988). An AC current is passed through the heating element to raise the temperature; this current is regulated by an analogue feedback circuit based a Chromel-Alumel thermocouple mounted underneath the heater strip using a gold rivet. Power is derived from a non-switching continuous full sine wave generator operating at 20 kHz (or 30 kHz). The heating system is able to heat samples to 700°C at constant heating rates from 0.1 to 20°C /s. Usually, N_2 is circulated in the measurement chamber during heating to avoid oxidation of the heating element at high temperatures (for coarse grains) and to avoid spurious TL (for fine grains). The temperature feedback system is designed to compensate for changes in thermal load from one sample to another (e.g. because of sample mass, or variations in gas flow).

However, it was recently discovered that the temperature control system of two models, the Risø TL/OSL-DA-15 and Risø TL/OSL-DA-15A readers, provides insufficient gain in the temperature feedback system. The objective of this note is to bring this to the users' attention (see section 'Hardware Upgrade'). Furthermore, we have improved the temperature calibration of the heating system and thereby reduced the systematic deviation between Actual temperature and Set temperature significantly (see section 'Software Upgrade').

Hardware Upgrade

Calibration of the temperature of the heater element is achieved by measuring the voltage across the thermocouple and adjusting the feedback loop-gain at 300°C and the off-set at 100°C. This temperature calibration is routinely carried out during manufacturing. However, because of the low loop-gain in these models the system does not always compensate fully for changes in gas flow. This is illustrated in Fig. 1 (filled circles) where an example of the deviation of the Actual temperature (the temperature directly determined from the thermocouple voltage) from the Set temperature (the temperature requested by the software) is shown as a function of the N_2 flow rate; the higher the flow rate the larger the deviation from the Set temperature of 300°C. If the N_2 flow rate is set to 1 L/min (the recommended flow rate for coarse grain work) the temperature of the heater plate is only 299°C. This offset is small compared to the thermal lag between heating element and the luminescence sample (see Jain et al. 2007; Betts et al. 1993) and is expected to be of little consequence to the majority of measurements. However, the magnitude of this effect will be dependent on the composition and concentration of the gas.

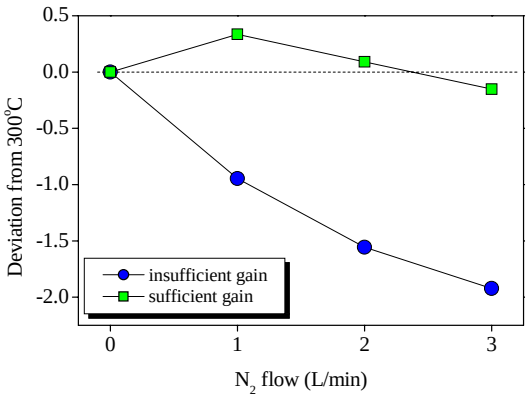

Figure 1: *The difference between Actual and Set temperature (for a Set temperature of 300°C) as a function of Nitrogen flow rate. The Actual temperature is measured using the thermocouple.*

Insufficient gain in the temperature feedback system may also affect the reproducibility of the Actual temperature. This was investigated by requesting a specific Set temperature (at a heating rate of 5°C/s) several times and then measuring the Actual temperature of the heater plate after it reached its equilibrium value. In Fig. 2 the deviation from the average Actual temperature is shown as a function of Set temperature (open circles). These measurements were carried out in the absence of a gas flow. The range of the temperature deviation is 2°C and the standard deviation of all of the measurements was 0.6°C.

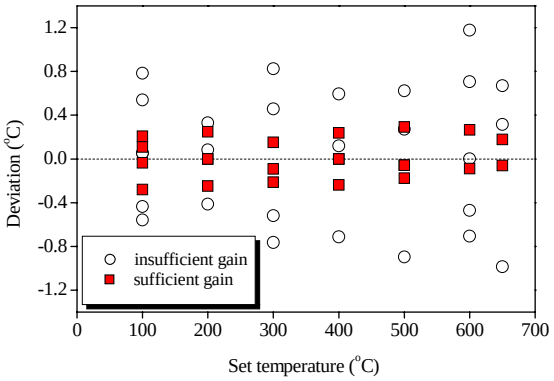

Figure 2: *Deviation around the mean as a function of Set temperature.*

In order to overcome this problem, the gain of the temperature feedback system is easily corrected by bypassing a single resistor on the control box motherboard. After this modification the temperature calibration must be readjusted (see footnotes). The effect of increasing the loop-gain is shown in Figure 1 and 2 (filled squares). The systematic effect on temperature as a function of flow rate is negligible and the reproducibility has improved significantly; the range of temperature deviation is reduced to 0.6°C and the standard deviation is reduced to 0.2°C.

Note, all these tests involve setting a fixed temperature and measuring the Actual temperature. The problem may be worse during heating, but we do not have dynamic data.

Software Upgrade

As mentioned above, temperature calibration during manufacturing is usually carried out at 300°C. Fig. 3a shows the Actual temperature reached after a short equilibration period as a function of Set temperature (heating rate of 5°C/s). In Fig. 3b (triangle symbols) the systematic deviation between Actual temperature and Set temperature is shown as a function of Set temperature. The deviation at 100°C is about -2°C and at 500°C it is about -4°C. This deviation is primarily related to electronic non-linearity; thermocouple non-linearity is negligible on this scale. All systematic deviations are within 2%. However, in the latest version of the MiniSys software (version 2.20 and upwards) it is now possible to correct for these systematic deviations (see Fig. 3b, circular symbols) by first measuring the deviations and then using a polynomial function to derive correction parameters. The resulting calibration is unique to each reader. After implementation of this software upgrade the systematic deviations are all within 0.25°C of the Set temperature.

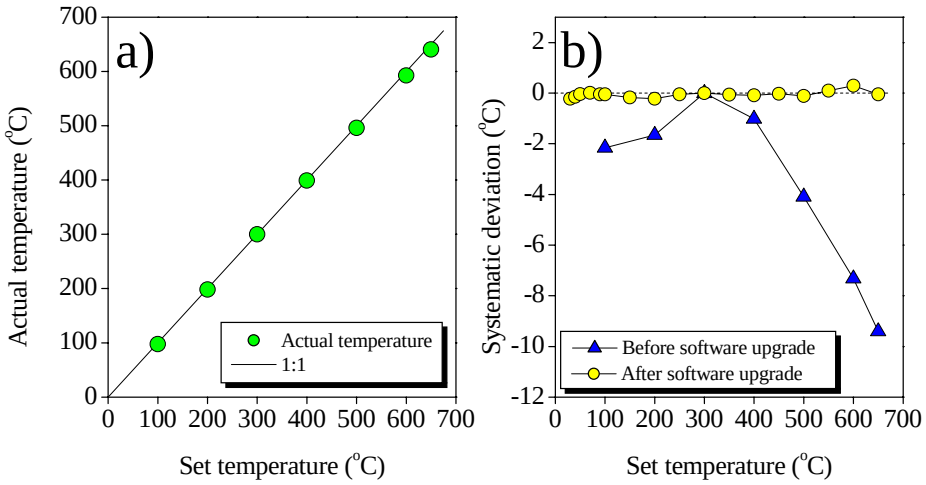

Figure 3: *a) Actual temperature as a function of Set temperature, b) Systematic deviation between Actual and Set temperature as a function of Set temperature.*

Summary
The deviations caused by the low loop-gain are all small compared to the temperatures involved and to the unavoidable variation in thermal contact between the heater plate and the phosphor. Nevertheless, the performance of all TL/OSL DA-15 and DA-15A readers can be slightly improved by modifying the control box's circuit board. Other models are not affected. Upgrading the software now allows the remaining small systematic errors in temperature to be reduced significantly; this software modification is relevant to all models controlled by a Mini-Sys.

How to upgrade
Further information on how to upgrade can be obtained by contacting either Kristina J. Thomsen (kristina.thomsen@risoe.dk) or Henrik E. Christiansen (henrik.christiansen@risoe.dk). Please accompany your enquiry with one photograph of the front plate, and one of the internal layout of the control box (please, remove the lid of the Control Box by unscrewing four screws).

Footnotes
1. All the above applies to heater circuits that have either not been modified or have been repaired at Risø. If the heater amplifier is replaced, the feedback circuit must be recalibrated.
2. The temperature display on the front of the MiniSys (all models) is for guidance only. This display uses an independent thermocouple preamplifier, and is not calibrated when the feedback circuit is set up. The only accurate method of checking the true thermocouple temperature is by direct measurement of the thermocouple voltage using a high impedance digital voltmeter (DVM).

References
Betts, D. S., Couturier, L., Khayrat, A. H., Luff, B. J., Townsend, P. D. (1993). Temperature distribution in thermoluminescence experiments. 1. Experimental results. *Journal of Physics D: Applied Physics* **26**, 843-848

Bøtter-Jensen, L. (1988). The automated Riso TL dating reader system. *Nuclear Tracks and Radiation Measurements* **14**, 177-188.

Jain M., Bøtter-Jensen, L., Murray, A. S., Essery, R. (2007). A peak structure in isothermal luminescence signals in Quartz: Origin and implications. *Journal of Luminescence* (in press)

Reviewer
G.A.T. Duller

Thesis Abstracts

Author: Matt Telfer
Thesis Title: Late Quaternary aeolian activity and palaeoenvironments of the southwestern Kalahari: Advances from an intensive chronometric investigation at Witpan, South Africa
Grade: PhD
Date: April 2007
Supervisor: David Thomas, Mark Bateman
Address: University of Sheffield, Department of Geography, UK

The southwestern Kalahari is a semi-arid dryland characterized by a range of landforms which have been interpreted as evidence of past environmental and climatic conditions different from those of today. These include currently inactive linear dunes, closed basins known locally as 'pans', and the crescentic lunette dunes which often accompany the pans on their lee side. However, palaeoenvironmental interpretation of these landforms has been hampered by incomplete understanding of their development and the difficulty in dating such sediments.

Witpan is an hourglass-shaped, 5 km long pan with a well-developed lunette dune, and is set amongst a linear dune field. This study applies a variety of physical and geochemical sedimentological analyses to the range of aeolian deposits found within the locale, set within a detailed timeframe provided by 113 Optically-Stimulated Luminescence (OSL) dates.

The current lunette at Witpan has accumulated predominantly within the past 2000 years, in a spatially complex manner reflecting differences in local sedimentary sources. The discovery of such complex sedimentation within a single landform has implications for future studies which attempt to use lunette sediments in palaeoenvironmental reconstruction. The linear dunes at Witpan are considered to respond primarily to variations in aridity forced by atmospheric circulation changes, and record sedimentary accumulation of different intensities dating back to around 100 ka. Most notable in the record is a period of particularly intense accumulation following the last glaciation, and culminating at around 9-16 ka. The Holocene has seen much reduced linear dune accumulation. The basin at Witpan contains a limited sedimentary record which is suggested to have accumulated during conditions wetter than those at present. The alkaline sediments are not conducive to the preservation of biogenic proxies, but OSL dating has potential for constraining a palaeoenvironmental record derived from physical and geochemical proxies.

Author: Helena Rodnight
Thesis Title: Developing a luminescence chronology for late Quaternary fluvial change in South African floodplain wetlands
Grade: PhD
Date: November 2006
Supervisor: Geoff Duller, Stephen Tooth
Address: Institute of Geography and Earth Sciences, University of Wales, Aberystwyth, UK

Owing to variation in the extent to which sediment grains transported in water are exposed to daylight, problems have been encountered in applying optically stimulated luminescence (OSL) dating to fluvial deposits. This thesis develops the OSL technique so that ages for heterogeneously-bleached fluvial samples can be derived based on the analysis of well-bleached grains. The ages calculated are then used to establish the timing and rates of different channel change processes. For two mixed bedrock-alluvial rivers with extensive floodplain wetlands located in the eastern Free State, South Africa, OSL sample collection was designed to investigate the lateral migration rates, meander cutoff ages, and avulsion frequency on the Klip River, and incision rate on the Schoonspruit.

Heterogeneous bleaching is evident in the majority of the samples and investigation shows that at least 50 equivalent dose (D_e) values are necessary to obtain reproducible dose distributions for these samples. Analysis of samples from palaeochannels of the Klip River demonstrates that the finite mixture model is the most appropriate for calculating the burial dose; replicate samples from the same palaeochannel reach give generally consistent ages, and comparison with radiocarbon ages for overlying organic-rich sediment gives good agreement. Using OSL dating, average lateral migration rates of ~0.05 and ~0.16 m/a over the last ~1.4 ka are obtained for

two meander bends on the Klip River, and five avulsions are identified as occurring since ~30 ka. On the Schoonspruit, the average incision rate has been ~2-3 mm/a since ~1.2 ka.

No clear link between these channel change processes and palaeoclimatic records from South Africa is evident. The results from this thesis, therefore, indicate that channel change processes on the Klip River and Schoonspruit result primarily from autogenic controls, rather than allogenic controls such as climate change.

Author: Christina Ankjaergaard
Thesis Title: Electron emission from natural minerals: Implications for charge movement and dosimetry
Grade: MSc
Date: September 2006
Supervisor: Andrew Murray
Address: Nordic Laboratory for Luminescence Dating, Department of Earth Sciences, Aarhus University, Risø National Laboratory, DK-4000 Roskilde, Denmark

Exo-electron signals from crystalline materials can be used to give insights into charge movement within crystals. This thesis investigates whether exo-electrons can be detected from natural insulating minerals such as quartz and feldspar, and uses comparisons with simultaneously measured luminescence to investigate the stimulation and recombination of charge trapped as a result of exposure to ionizing radiation. These investigations lead to a consideration of the potential use of these exo-electron signals for measurement of absorbed doses in retrospective dosimetry.

A Geiger-Müller electron detector was developed for this work as an attachment to the existing automated Risø TL/OSL reader, such that thermally and optically stimulated electron emission and luminescence can be detected simultaneously, and sample treatment (i.e. irradiation, heating, light stimulation) undertaken without moving the sample from the detector volume. Using this equipment, both thermally and optically stimulated luminescence (TL, OSL) and exo-electron emission (TSE, OSE) were recorded from common salt, quartz and feldspar. An experiment is described which allows the conclusion that the dosimetric behavior of surface traps and bulk traps is indistinguishable. This simplifies the interpretation of the comparison of exo-electron (surface) with luminescence (bulk and surface) phenomena. Using quartz and feldspar, the relative OSE and OSL dose response is then examined, followed by the relative thermal stability of the two signals from quartz. In a preliminary comparison of infrared stimulated signals from feldspar, it was found that the OSE signal was not detectable, despite a strong OSL signal. These results are discussed in terms of published models of charge movement in quartz and feldspar.

Occasional unstable detector behavior gave rise to infrequent noise pulses in the exo-electron data. This led to a redesign of the detector and electronics. The new design gave an improvement in sensitivity of 10 to 20 times, and allowed a preliminary study of the OSE characteristics of more exotic materials such as paper, cotton, keratin, and coral. To confirm the validity of the most important earlier results, experiments on the thermal stability of quartz, and the effect of prior infrared stimulation on feldspar were revisited in more detail.

The use of exo-electron signals in retrospective dosimetry and the possible advantages they offer compared to luminescence were investigated by simultaneous measurement of exo-electron and luminescence dose response curves from different samples, (i) to illustrate the large variability in relative behavior between these curves, and (ii) to determine how the growth curve shape depends on preheat temperature. After these initial examinations, exo-electron emission and luminescence dose recovery tests using quartz were used to demonstrate that dose given before any laboratory heating could be measured accurately. Finally, preliminary investigations of the use of natural exo-electron signals in chronometry are presented. This important potential application is illustrated by an example showing the use of OSE to estimate a natural dose which could not be measured using OSL.

It is concluded that exo-electron signals from natural minerals can be measured easily, are stable in time, and survive aggressive chemical surface cleaning. Together with luminescence signals, they can be used to provide important new insights into charge movement in insulators, and seem to have considerable potential application in both accident dosimetry and chronometry.

Author: Mirko Ballarini
Thesis Title: Optical dating of quartz from young deposits – from single-aliquot to single-grain
Grade: PhD
Date: May 2006
Supervisor: Jakob Wallinga, Adrie Bos
Address: Netherlands Centre for Luminescence Dating, Delft University of Technology, The Netherlands

Optically Stimulated Luminescence (OSL) dating showed to be a robust and reliable tool for dating quartz samples in the age range of 1,000 up to 150,000 years. However, optical dating below and beyond these limits remains a challenge. OSL dating relies on the assumption that the luminescence signal of grains is fully reset to zero by sunlight exposure before deposition. If this requirement is not fulfilled (i.e. grains were "poorly-bleached"), ages may be grossly overestimated. In particular, poor-bleaching can significantly affect age estimations of young sediments, for which the remnant signal may be large relative to the signal built up during burial. One way to investigate poor-bleaching within a sample is to measure the OSL signal from individual grains rather than from aliquots made up of several thousands of grains.

The aim of this thesis is to determine the feasibility of optical dating techniques to individual grains of quartz from deposits formed within the last 300 years.

The standard single-aliquot (SA) technique has been validated on aeolian coastal-dune quartz samples, for which heterogeneous bleaching was not a significant issue. This gave us knowledge of the limits of standard luminescence techniques. The study site is the south-west of the island of Texel (The Netherlands), whose development of sand-dune deposits for the last 300 years is very well documented by means of maps. It was found that aeolian samples as young as 10 years old could be dated by quartz single-aliquot dating. One sample (<1 yr), which was known to have experienced poor-bleaching before deposition, gave an OSL age of 73±24 years, making it a good candidate for further single-grain (SG) analysis.

Before attempting any sort of SG age estimation, we focused at improving both instrumentation and dating procedures. This need arose from the fact that luminescence signals from young samples are weak and noisy. We found that the light detection efficiency can be increased by choosing an alternative set of detection filters to be used with the photomultiplier tube. As a result, a greater percentage of grains could be used for our analysis. We also investigated the homogeneity of our beta-sources, finding that for two sources out of four the irradiation of sample disks was not uniform. This could be seen from 3-D graphs, where the dose rate delivered to each individual grain was plotted against the position of the grain on the disk.

The single-aliquot-regenerative (SAR) protocol, commonly used in single-aliquot quartz measurements, was also modified to be used on individual quartz grains. The most important changes were focused on two issues: a) further increase of the percentage of grains that could be accepted for dose analysis and b) selection of the OSL component that is more representative of the last depositional event that is to be dated. We tested this protocol on two well-bleached samples of 300 years, previously dated by single-aliquot means. We found that SG ages were comparable to SA ages if our modified SAR protocol was used.

Such a modified protocol was finally applied on two more samples from Texel, one being less than one year old and the other the 73-year-old sample whose age was overestimated by standard single-aliquot methods. With the first sample we tested our ability to date extremely young individual grains; with the second, our ability to cope with poor bleaching occurred to young quartz grains. We found that the zero-age sample could be correctly dated (within errors) but very large uncertainties are associated with the final dose. For the poorly-bleached sample, no satisfactory dose estimate could be provided. However, in this last case, poorly-bleached grains responsible for the SA age overestimation could be identified.

The work presented in this thesis shows the feasibility and great potential of SG dating of young quartz samples – and a suitable protocol is proposed. Despite encouraging results further investigations and additional innovative approaches are needed in order to make optical single-grain dating a robust and reliable tool.

Bibliography
Compiled by Ann Wintle

From 1st October 2006 to 31st May 2007

Aagaard, T., Orford, J., and Murray, A. S. (2007). Environmental controls on coastal dune formation; Skallingen Spit, Denmark. *Geomorphology* **83,** 29-47.

Alexanderson, H. (2007). Residual OSL signals from modern Greenlandic river sediments. *Geochronometria* **26,** 1-9.

Amit, R., Lekach, J., Ayalon, A., Porat, N., and Grodek, T. (2007). New insight into pedogenic processes in extremely arid environments and their paleoclimatic implications-the Negev Desert, Israel. *Quaternary International* **162-163,** 61-75.

Anikovich, M. V., Sinitsyn, A. A., Hoffecker, J. F., Holliday, V. T., Popov, V. V., Lisitsyn, S. N., Forman, S. L., Levkovskaya, G. M., Pospelova, G. A., Kuz'mina, I. E., Burova, N. D., Goldberg, P., Macphail, R. I., Giaccio, B., and Praslov, N. D. (2007). Early Upper Paleolithic in Eastern Europe and implications for the dispersal of modern humans. *Science* **315,** 223-226.

Ankjaergaard, C., and Murray, A. S. (2007). Total beta and gamma dose rates in trapped charge dating based on beta counting. *Radiation Measurements* **42,** 352-359.

Armitage, S. J., Botha, G. A., Duller, G. A. T., Wintle, A. G., Rebelo, L. P., and Momade, F. J. (2006). The formation and evolution of the barrier islands of Inhaca and Bazaruto, Mozambique. *Geomorphology* **82,** 295-308.

Avni, Y., Porat, N., Plakht, J., and Avni, G. (2006). Geomorphic changes leading to natural desertification versus anthropogenic land conservation in an arid environment, the Negev Highlands, Israel. *Geomorphology* **82,** 177-200.

Ballarini, M., Wallinga, J., Wintle, A. G., and Bos, A. J. J. (2007). A modified SAR protocol for optical dating of individual grains from young quartz samples. *Radiation Measurements* **42,** 360-369.

Bateman, M. D., Boulter, C. H., Carr, A. S., Frederick, C. D., Peter, D., and Wilder, M. (2007). Preserving the palaeoenvironmental record in Drylands: Bioturbation and its significance for luminescence-derived chronologies. *Sedimentary Geology* **195,** 5-19.

Beveridge, C., Kocurek, G., Ewing, R. C., Lancaster, N., Morthekai, P., Singhvi, A. K., and Mahan, S. A. (2006). Development of spatially diverse and complex dune-field patterns: Gran Desierto Dune Field, Sonora, Mexico. *Sedimentology* **53,** 1391-1409.

Blair, M. W., Kalchgruber, R., and McKeever, S. W. S. (2007). Developing luminescence dating for extraterrestrial applications: Characterization of martian simulants and minerals. *Radiation Measurements* **42,** 392-399.

Botha, G., and Porat, N. (2007). Soil chronosequence development in dunes on the southeast African coastal plain, Maputaland, South Africa. *Quaternary International* **162-163,** 111-132.

Bristow, C. S., Duller, G. A. T., and Lancaster, N. (2007). Age and dynamics of linear dunes in the Namib Desert. *Geology* **35,** 555-558.

Buynevich, I. V., FitzGerald, D. M., and Goble, R. J. (2007). A 1500 yr record of North Atlantic storm activity based on optically dated relict beach scarps. *Geology* **35,** 543-546.

Chandra, S., Rhodes, E., and Richards, K. (2007). Luminescence dating of late Quaternary fluvial sediments in the Rapti Basin, north-central Gangetic plains. *Quaternary International* **159,** 47-56.

Chase, B. M., and Thomas, D. S. G. (2006). Late Quaternary dune accumulation along the western margin of South Africa: distinguishing forcing mechanisms through the analysis of migratory dune forms. *Earth and Planetary Science Letters* **251,** 318-333.

Chase, B. M., and Thomas, D. S. G. (2007). Multiphase late Quaternary aeolian sediment accumulation in western South Africa: Timing and relationship to palaeoclimatic changes inferred from the marine record. *Quaternary International* **166,** 29-41.

Chase, P. G., Debenath, A., Dibble, H. L., McPherron, S. P., Schwarcz, H. P., Stafford, J. T. W., and Tournepiche, J.-F. (2007). New dates for the Fontechevade (Charente, France) Homo remains. *Journal of Human Evolution* **52,** 217-221.

Chithambo, M. L. (2007). The analysis of time-resolved optically stimulated luminescence: I. Theoretical considerations. *Journal of Physics D-Applied Physics* **40,** 1874-1879.

Chithambo, M. L. (2007). The analysis of time-resolved optically stimulated luminescence: II. Computer simulations and experimental results. *Journal of Physics D-Applied Physics* **40,** 1880-1889.

Chithambo, M. L., Preusser, F., Ramseyer, K., and Ogundare, F. O. (2007). Time-resolved luminescence of low sensitivity quartz from crystalline rocks. *Radiation Measurements* **42,** 205-212.

Clarke, M. L., Milodowski, A. E., Bouch, J. E., Leng, M. J., and Northmore, K. J. (2007). New OSL dating of UK loess: indications of two phases of Late Glacial dust accretion in SE England and climate implications. *Journal of Quaternary Science* **22,** 361-371.

Clemmensen, L. B., Pedersen, K., Murray, A., and Heinemeier, J. (2006). A 7000-year record of coastal evolution, Vejers, SW Jutland, Denmark. *Bulletin of the Geological Society of Denmark* **53,** 1-22.

Cox, R. T., Cherryhomes, J., Harris, J. B., Larsen, D., Van Arsdale, R. B., and Forman, S. L. (2006). Paleoseismology of the southeastern Reelfoot Rift in western Tennessee and implications for intraplate fault zone evolution. *Tectonics* **25,** TC3019.

Cupper, M. L., and Duncan, J. (2006). Last glacial megafaunal death assemblage and early human occupation at Lake Menindee, southeastern Australia. *Quaternary Research* **66,** 332-341.

Davidson, A. T., Valberg, L., Townsend, P. D., Kozakiewicz, A. G., Derry, T. E., Comins, J. D., and Suszynska, M. (2006). The effect of impurities on TL emission wavelengths of NaCl crystals. *Nuclear Instruments and Methods in Physics Research Section B:* **250,** 354-358.

De Carvalho, G. S., Granja, H. M., Loureiro, E., and Henriques, R. (2006). Late Pleistocene and Holocene environmental changes in the coastal zone of northwestern Portugal. *Journal of Quaternary Science* **21,** 859-877.

De Corte, F., Vandenberghe, D., Hossain, S. M., De Wispelaere, A., Buylaert, J. P., and Van den Haute, P. (2007). Preparation and characterization of loess sediment for use as a reference material in the annual radiation dose determination for luminescence dating. *Journal of Radioanalytical and Nuclear Chemistry* **272,** 311-319.

DeLong, S. B., Pelletier, J. D., and Arnold, L. (2007). Bedrock landscape development modeling: Calibration using field study, geochronology, and digital elevation model analysis. *Geological Society of America Bulletin* **119,** 157-173.

Dobosz, B., and Krzyminiewski, R. (2007). Characteristic of paramagnetic centres in burnt clay and pottery by the EPR method. *Radiation Measurements* **42,** 213-219.

D'Oca, M. C., Bartolotta, A., Cammilleri, M. C., Brai, M., Marrale, M., Triolo, A., and Parlato, A. (2007). Qualitative and quantitative thermoluminescence analysis on irradiated oregano. *Food Control* **18,** 996-1001.

Duller, G. A. T. (2006). Comment on "Human footprints in Central Mexico older than 40,000 years" by S. Gonzalez, D. Huddart, M.R. Bennett and A. Gonzalez-Huesca. *Quaternary Science Reviews* **25,** 3074-3076.

Duller, G. A. T. (2006). Single grain optical dating of glacigenic deposits. *Quaternary Geochronology* **1,** 296-304.

Engin, B. (2007). Thermoluminescence parameters and kinetics of irradiated inorganic dust collected from black peppers. *Food Control* **18,** 243-250.

Eriksson, M. G., Olley, J. M., Kilham, D. R., Pietsch, T., and Wasson, R. J. (2006). Aggradation and incision since the very late Pleistocene in the Naas River, south-eastern Australia. *Geomorphology* **81,** 66-88.

Fattahi, M., Walker, R. T., Khatib, M. M., Dolati, A., and Bahroudi, A. (2007). Slip-rate estimate and past earthquakes on the Doruneh fault, eastern Iran. *Geophysical Journal International* **168,** 691-709.

Feathers, J. K., Rhodes, E. J., Huot, S., and McAvoy, J. M. (2006). Luminescence dating of sand deposits related to late Pleistocene human occupation at the Cactus Hill Site, Virginia, USA. *Quaternary Geochronology* **1,** 167-187.

Forman, S. L., Pierson, J., Gomez, J., Brigham-Grette, J., Nowaczyk, N. R., and Melles, M. (2007). Luminescence geochronology for sediments from Lake El'gygytgyn, northeast Siberia, Russia: constraining the timing of paleoenvironmental events for the past 200 ka. *Journal of Paleolimnology* **37,** 77-88.

French, H. M., Demitroff, M., Forman, S. L., and Newell, W. L. (2007). A chronology of Late-Pleistocene permafrost events in southern New Jersey, eastern USA. *Permafrost and Periglacial Processes* **18,** 49-59.

Friis, H., Finch, A. A., Townsend, P. D., Hole, D. E., and El Mkami, H. (2007). Ionoluminescence of leucophanite. *American Mineralogist* **92,** 254-260.

Fuchs, M. (2007). An assessment of human versus climatic impacts on Holocene soil erosion in NE Peloponnese, Greece. *Quaternary Research* **67,** 349-356.

Fujita, H., and Hashimoto, T. (2007). Effects of annealing temperatures on some radiation-induced phenomena in natural quartz. *Radiation Measurements* **42,** 156-162.

Giannini, P. C. F., Sawakulchi, A. O., Martinho, C. T., and Tatumi, S. H. (2007). Eolian depositional episodes controlled by Late Quaternary relative sea level changes on the Imbituba-Laguna coast (southern Brazil). *Marine Geology* **237,** 143-168.

Giosan, L., Donnelly, J. P., Constantinescu, S., Filip, F., Ovejanu, I., Vespremeanu-Stroe, A., Vespremeanu, E., and Duller, G. A. T. (2006). Young Danube delta documents stable Black Sea level since the middle Holocene. Morphodynamic, paleogeographic, and archaeological implications. *Geology* **34,** 757-760.

Göksu, H. Y., Stepanenko, V. F., Bailiff, I. K., and Jungner, H. (2006). Intercomparison of luminescence measurements of bricks from Dolon' Village: Experimental methodology and results of European study group. *Journal of Radiation Research* **47,** A29-A37.

Gomez-Ros, J. M., Furetta, C., Cruz-Zaragoza, E., Lis, M., Torres, A., and Monsivais, G. (2006). Dose dependence and thermal stability of the thermoluminescence emission in inorganic dust from mint and camomile. *Nuclear Instruments & Methods in Physics Research A* **566,** 727-732.

Grine, F. E., Bailey, R. M., Harvati, K., Nathan, R. P., Morris, A. G., Henderson, G. M., Ribot, I., and Pike, A. W. G. (2007). Late Pleistocene human skull from Hofmeyr, South Africa, and modern human origins. *Science* **315,** 226-229.

Grün, R. (2006). Direct dating of human fossils. *Yearbook of Physical Anthropology* **49,** 2-48.

Guerin, G., and Gillot, P. Y. (2007). New elements of chronology of 'Bas Vivarais' Pleistocene volcanism (Ardeche, France) by thermoluminescence dating. *Comptes Rendus Geoscience* **339,** 40-49.

Hall, A. M., Hansom, J. D., Williams, D. M., and Jarvis, J. (2006). Distribution, geomorphology and lithofacies of cliff-top storm deposits: Examples from the high-energy coasts of Scotland and Ireland. *Marine Geology* **232,** 131-155.

Hashimoto, T., Yanagawa, Y., and Yawata, T. (2007). Blue and red thermoluminescence of natural quartz in the temperature region from -196 to 400°C. *Radiation Measurements* **42,** 341-346.

Holbrook, J., Autin, W. J., Rittenour, T. M., Marshak, S., and Goble, R. J. (2006). Stratigraphic evidence for millennial-scale temporal clustering of earthquakes on a continental-interior fault: Holocene Mississippi River floodplain deposits, New Madrid seismic zone, USA. *Tectonophysics* **420,** 431-454.

Hollands, C. B., Nanson, G. C., Jones, B. G., Bristow, C. S., Price, D. M., and Pietsch, T. J. (2006). Aeolian-fluvial interaction: evidence for Late Quaternary channel change and wind-rift linear dune formation in the northwestern Simpson Desert, Australia. *Quaternary Science Reviews* **25,** 142-162.

Holliday, V. T., Hoffecker, J. F., Goldberg, P., Macphail, R. I., Forman, S. L., Anikovich, M., and Sinitsyn, A. (2007). Geoarchaeology of the Kostenki-Borshchevo sites, Don River Valley. *Geoarchaeology* **22,** 181-228.

Holliday, V. T., Huckell, B. B., Mayer, J. H., Forman, S. L., and McFadden, L. D. (2006). Geoarchaeology of the Boca Negra Wash area, Albuquerque Basin, New Mexico, USA. *Geoarchaeology* **21,** 765-802.

Holliday, V. T., Kring, D. A., Mayer, J. H., and Goble, R. J. (2005). Age and effects of the Odessa meteorite impact, western Texas, USA. *Geology* **33,** 945-948.

Huang, C. C., Jia, Y. F., Pang, J. L., Zha, X. C., and Su, H. X. (2006). Holocene colluviation and its implications for tracing human-induced soil erosion and redeposition on the piedmont loess lands of the Qinling Mountains, northern China. *Geoderma* **136,** 838-851.

Huntley, D. J., Baril, M. R., and Haidar, S. (2007). Tunnelling in plagioclase feldspars. *Journal of Physics D-Applied Physics* **40,** 900-906.

Ivannikov, A., Zhumadilov, K., Tieliewuhan, E., Jiao, L., Zharlyganova, D., Apsalikov, K. N., Berekenova, G., Zhumadilov, Z., Toyoda, S., Miyazawa, C., Skvortsov, V., Stepanenko, V., Endo, S., Tanaka, K., and Hoshi, M. (2006). Results of EPR dosimetry for population in the vicinity of the most contaminating radioactive fallout trace after the first nuclear test in the Semipalatinsk test site. *Journal of Radiation Research* **47,** A39-A46.

Jain, M., Bøtter-Jensen, L., and Thomsen, K. J. (2007). High local ionization density effects in x-ray excitations deduced from optical stimulation of trapped charge in Al_2O_3:C. *Journal of Physics: Condensed Matter* **19,** doi:10.1088/0953-8984/19/11/116201.

Kaiser, K., Barthetmes, A., Pap, S. C., Hilgers, A., Janke, W., Kuhn, P., and Theuerkauf, M. (2006). A Lateglacial palaeosol cover in the Altdarss area, southern Baltic Sea coast (northeast Germany): investigations on pedology, geochronology and botany. *Netherlands Journal of Geosciences-Geologie En Mijnbouw* **85,** 197-220.

Kindermann, K., Bubenzer, O., Nussbaum, S., Riemer, H., Darius, F., Pollath, N., and Smettan, U. (2006). Palaeoenvironment and Holocene land use of Djara, western desert of Egypt. *Quaternary Science Reviews* **25,** 1619-1637.

Kitis, G., Polymeris, G. S., Pagonis, V., and Tsirliganis, N. C. (2006). Thermoluminescence response and apparent anomalous fading factor of Durango fluorapatite as a function of the heating rate. *Physica Status Solidi a* **203,** 3816-3823.

Kiyak, N. G., Polymeris, G. S., and Kitis, G. (2007). Component resolved OSL dose response and sensitization of various sedimentary quartz samples. *Radiation Measurements* **42,** 144-155.

Kjaer, K. H., Lagerlund, E., Adrielsson, L., Thomas, P. J., Murray, A., and Sandgren, P. (2006). The first independent chronology for Middle and Late Weichselian sediments from southern Sweden and the Island of Bornholm. *Gff* **128,** 209-220.

Klasen, N., Fiebig, M., Preusser, F., Reitner, J. M., and Radtke, U. (2007). Luminescence dating of proglacial sediments from the Eastern Alps. *Quaternary International* **164-165,** 21-32.

Kocurek, G., Carr, M., Ewing, R., Havholm, K. G., Nagar, Y. C., and Singhvi, A. K. (2007). White Sands Dune Field, New Mexico: Age, dune dynamics and recent accumulations. *Sedimentary Geology* **197,** 313-331.

Kumar, R., Suresh, N., Sangode, S. J., and Kumaravel, V. (2007). Evolution of the Quaternary alluvial fan system in the Himalayan foreland basin: Implications for tectonic and climatic decoupling. *Quaternary International* **159,** 6-20.

Lai, Z., Wintle, A. G., and Thomas, D. S. G. (2007). Rates of dust deposition between 50 ka and 20 ka revealed by OSL dating at Yuanbao on the Chinese Loess Plateau. *Palaeogeography, Palaeoclimatology, Palaeoecology* **248,** 431-439.

Liu, G., Zhang, X., Cui, Z., Wu, Y., and Ju, Y. (2006). A review of glacial sequences of the Kunlun Pass, northern Tibetan Plateau. *Quaternary International* **154-155,** 63-72.

Lu, Y. C., Wang, X. L., and Wintle, A. G. (2007). A new OSL chronology for dust accumulation in the last 130,000 yr for the Chinese Loess Plateau. *Quaternary Research* **67,** 152-160.

Mahan, S. A., Miller, D. M., Menges, C. M., and Yount, J. C. (2007). Late Quaternary stratigraphy and luminescence geochronology of the northeastern Mojave Desert. *Quaternary International* **166,** 61-78.

Maroulis, J. C., Nanson, G. C., Price, D. M., and Pietsch, T. (2007). Aeolian-fluvial interaction and climate change: source-bordering dune development over the past ~100 ka on Cooper Creek, central Australia. *Quaternary Science Reviews* **26,** 386-404.

Mauz, B., and Bungenstock, F. (2007). How to reconstruct trends of late Holocene relative sea level: A new approach using tidal flat clastic sediments and optical dating. *Marine Geology* **237,** 225-237.

Meltzner, A. J., Rockwell, T. K., and Owen, L. A. (2006). Recent and long-term behavior of the Brawley fault zone, Imperial Valley, California: An escalation in slip rate? *Bulletin of the Seismological Society of America* **96,** 2304-2328.

Mercier, N., Valladas, H., Froget, L., Joron, J. L., Reyss, J. L., Weiner, S., Goldberg, P., Meignen, L., Bar-Yosef, O., Belfer-Cohen, A., Chech, M., Kuhn, S. L., Stiner, M. C., Tillier, A. M., Arensburg, B., and Vandermeersch, B. (2007). Hayonim Cave: a TL-based chronology for this Levantine Mousterian sequence. *Journal of Archaeological Science* **34,** 1064-1077.

Miallier, D., Sanzelle, S., Pilleyre, T., and Bassinet, C. (2006). Residual thermoluminescence for sun-bleached quartz: Dependence on pre-exposure radiation dose. *Quaternary Geochronology* **1,** 313-319.

Miao, X., Mason, J. A., Johnson, W. C., and Wang, H. (2007). High-resolution proxy record of Holocene climate from a loess section in Southwestern Nebraska, USA. *Palaeogeography, Palaeoclimatology, Palaeoecology* **245,** 368-381.

Miao, X. D., Mason, J. A., Swinehart, J. B., Loope, D. B., Hanson, P. R., Goble, R. J., and Liu, X. D. (2007). A 10,000 year record of dune activity, dust storms, and severe drought in the central Great Plains. *Geology* **35,** 119-122.

Molodkov, A., Jaek, I., and Vasilchenko, V. (2007). Anomalous fading of IR-stimulated luminescence from feldspar minerals: some results of the study. *Geochronometria* **26,** 11-17.

Murari, M. K., Achyuthan, H., and Singhvi, A. K. (2007). Luminescence studies on the sediments laid down by the December 2004 tsunami event: Prospects for the dating of palaeo tsunamis and for the estimation of sediment fluxes. *Current Science* **92,** 367-371.

Nakata, Y., Tamaki, M., and Hashimoto, T. (2007). Red-thermoluminescence dating using quartz grains extracted from a roof-tile of an old Japanese temple. *Journal of Radioanalytical and Nuclear Chemistry* **272,** 433-438.

Navarro-Gonzalez, R., Mahan, S. A., Singhvi, A. K., Navarro-Aceves, R., Rajot, J. L., McKay, C. P., Coll, P., and Raulin, F. (2007). Paleoecology reconstruction from trapped gases in a fulgurite from the late Pleistocene of the Libyan Desert. *Geology* **35,** 171-174.

Newnham, R. M., Vandergoes, M. J., Hendy, C. H., Lowe, D. J., and Preusser, F. (2007). A terrestrial palynological record for the last two glacial cycles from southwestern New Zealand. *Quaternary Science Reviews* **26,** 517-535.

Nielsen, A., Murray, A. S., Pejrup, M., and Elberling, B. (2006). Optically stimulated luminescence dating of a Holocene beach ridge plain in Northern Jutland, Denmark. *Quaternary Geochronology* **1,** 305-312.

Ninagawa, K., Imae, N., Kojima, H., Yanai, K., and Jull, A. J. T. (2006). Thermoluminescence study in the Japanese Antarctic meteorites collection: Asuka ordinary chondrites. *Meteoritics & Planetary Science* **41,** A132-A132.

Ogundare, F., and Chithambo, M. L. (2007). Thermoluminescence kinetic analysis of quartz with a glow peak that shifts in an unusual manner with irradiation dose. *Journal of Physics D: Applied Physics* **40,** 247-253.

Ormo, J., Koeberl, C., Rossi, A. P., and Komatsu, G. (2006). Geological and geochemical data from the proposed Sirente crater field: New age dating and evidence for heating of target. *Meteoritics & Planetary Science* **41,** 1331-1345.

Owen, L. A., Bright, J., Finkel, R. C., Jaiswal, M. K., Kaufman, D. S., Mahan, S., Radtke, U., Schneider, J. S., Sharp, W., Singhvi, A. K., and Warren, C. N. (2007). Numerical dating of a Late Quaternary spit-shoreline complex at the northern end of Silver Lake playa, Mojave Desert, California: A comparison of the applicability of radiocarbon, luminescence, terrestrial cosmogenic nuclide, electron spin resonance, U-series and amino acid racemization methods. *Quaternary International* **166,** 87-110.

Pagonis, V., Chen, R., and Wintle, A. G. (2007). Modelling thermal transfer in optically stimulated luminescence of quartz. *Journal of Physics D-Applied Physics* **40,** 998-1006.

Pan, B. T., Gao, H. S., Wu, G. J., Li, J. J., Li, B. Y., and Ye, Y. G. (2007). Dating of erosion surface and terraces in the eastern Qilian Shan, northwest China. *Earth Surface Processes and Landforms* **32,** 143-154.

Pedoja, K., Dumont, J. F., Lamothe, M., Ortlieb, L., Collot, J. Y., Ghaleb, B., Auclair, M., Alvarez, V., and Labrousse, B. (2006). Plio-Quaternary uplift of the Manta Peninsula and La Plata Island and the subduction of the Carnegie Ridge, central coast of Ecuador. *Journal of South American Earth Sciences* **22,** 1-21.

Preusser, F., Blei, A., Graf, H. R., and Schlüchter, C. (2007). Luminescence dating of Würmian (Weichselian) proglacial sediments from Switzerland: methodological aspects and stratigraphical conclusions. *Boreas***,** 130-142.

Preusser, F., and Degering, D. (2007). Luminescence dating of the Niederweningen mammoth site, Switzerland. *Quaternary International* **164-165,** 106-112.

Prideaux, G. J., Long, J. A., Ayliffe, L. K., Hellstrom, J. C., Pillans, B., Boles, W. E., Hutchinson, M. N., Roberts, R. G., Cupper, M. L., Arnold, L. J., Devine, P. D., and Warburton, N. M. (2007). An arid-adapted middle Pleistocene vertebrate fauna from south-central Australia. *Nature* **445,** 422-425.

Prideaux, G. J., Roberts, R. G., Megirian, D., Westaway, K. E., Hellstrom, J. C., and Olley, J. M. (2007). Mammalian responses to Pleistocene climate change in southeastern Australia. *Geology* **35,** 33-36.

Rasheedy, M. S., and Abd-Elmageed, A. I. (2007). The validity of the two heating rates method to obtain the trapping parameters from general-order thermoluminescence glow peaks. *Journal of Physics and Chemistry of Solids* **68,** 243-248.

Reinhardt, E. G., Goodman, B. N., Boyce, J. I., Lopez, G., van Hengsturn, P., Rink, W. J., Mart, Y., and Raban, A. (2006). The tsunami of 13 December A.D. 115 and the destruction of Herod the Great's harbor at Caesarea Maritima, Israel. *Geology* **34,** 1061-1064.

Rhodes, E. J. (2007). Quartz single grain OSL sensitivity distributions: implications for multiple grain single aliquot dating. *Geochronometria* **26,** 19-29.

Richter, D., and Krbetschek, M. (2006). A new thermoluminescence dating technique for heated flint. *Archaeometry* **48,** 695-705.

Richter, D., Mercier, N., Valladas, H., Jaubert, J., Texier, P. J., Brugal, J. P., Kervazo, B., Reyss, J. L., Joron, J. L., and Wagner, G. A. (2007). Thermoluminescence dating of heated flint from the Mousterian site of Berigoule, Murs, Vaucluse, France. *Journal of Archaeological Science* **34,** 532-539.

Rigaud, J.-P., Texier, P.-J., Parkington, J., and Poggenpoel, C. (2006). Le mobilier Stillbay et Howiesons Poort de l'abri Diepkloof. La chronologie du Middle Stone Age sud-africain et ses implications. *Comptes Rendus Palevol* **5,** 839-849.

Rittenour, T. M., Blum, M. D., and Goble, R. J. (2007). Fluvial evolution of the lower Mississippi River valley during the last 100 k.y. glacial cycle: Response to glaciation and sea-level change. *Bulletin of the Geological Society of America* **119,** 586-608.

Sanchez-Munoz, L., Garcia-Guinea, J., Correcher, V., and Delgado, A. (2007). Thermally stimulated power law relaxation of radiation-induced defects in K-feldspar. *Journal of Physics-Condensed Matter* **19,** doi:10.1088/0953-8984/19/4/046202.

Schwenninger, J.-L., Gonzalez, S., Huddart, D., Bennett, M., and Gonzalez-Huesca, A. (2006). The OSL dating of the Xalnene ash: A reply to comments by G. Duller on "Human footprints in Central Mexico older than 40,000 years". *Quaternary Science Reviews* **25,** 3077-3080.

Shaw, P. A., and Bateman, M. D. (2006). Provenance and chronology of the Barcavecchia Tufa, Southwest Etna, Sicily. *Bollettino Della Societa Geologica Italiana* **125,** 265-272.

Simoes, M., Avouac, J. P., Chen, Y.-G., Singhvi, A. K., Wang, C.-Y., Jaiswal, M., Chan, Y.-C., and Bernard, S. (2007). Kinematic analysis of the Pakuashan fault tip fold, west central Taiwan: Shortening rate and age of folding inceprion. *Journal of Geophysical Research* **112,** B03S14, doi:10.1029/2005JB004198.

Singh, S., Parkash, B., Rao, M. S., Arora, M., and Bhosle, B. (2006). Geomorphology, pedology and sedimentology of the Deoha/Ganga-Ghaghara Interfluve, Upper Gangetic Plains (Himalayan foreland basin) - extensional tectonic implications. *Catena* **67,** 183-203.

Sohn, M. F., Mahan, S. A., Knott, J. R., and Bowman, D. D. (2007). Luminescence ages for alluvial-fan deposits in Southern Death Valley: Implications for climate-driven sedimentation along a tectonically active mountain front. *Quaternary International* **166,** 49-60.

Soressi, M., Jones, H. L., Rink, W. J., Maureille, B., and Tillier, A. M. (2007). The Pech-de-l'Aze I Neandertal child: ESR, uranium-series, and AMS ^{14}C dating of its MTA type B context. *Journal of Human Evolution* **52,** 455-466.

Stepanenko, V. F., Hoshi, M., Bailiff, I. K., Ivannikov, A. I., Toyoda, S., Yamamoto, M., Simon, S. L., Matsuo, M., Kawano, N., Zhumadilov, Z., Sasaki, M. S., Rosenson, R. I., and Apsalikov, K. N. (2006). Around Semipalatinsk nuclear test site: Progress of dose estimations relevant to the consequences of nuclear tests. *Journal of Radiation Research* **47,** A1-A13.

Stepanenko, V. F., Hoshi, M., Dubasov, Y. V., Sakaguchi, A., Yamamoto, M., Orlov, M. Y., Bailiff, I. K., Ivannikov, A. I., Skvortsov, V. G., Iaskova, E. K., Kryukova, I. G., Zhumadilov, K. S., Endo, S., Tanaka, K., Apsalikov, K. N., and Gusev, B. I. (2006). A gradient of radioactive contamination in Dolon village near the SNTS and comparison of computed dose values with instrumental estimates for the 29 August, 1949 nuclear test. *Journal of Radiation Research* **47,** A149-A158.

Stevens, T., Thomas, D. S. G., Armitage, S. J., Lunn, H. R., and Lu, H. (2007). Reinterpreting climate proxy records from late Quaternary Chinese loess: A detailed OSL investigation. *Earth-Science Reviews* **80,** 111-136.

Sunta, C. M., Kumar, M., Kher, R. K., and Bhatt, B. C. (2006). Thermoluminescence emission from localized recombination model. *Journal of Physics D-Applied Physics* **39,** 4557-4562.

Tanir, G., and Bolukdemir, M. H. (2006). Activation energy of NaCl as a function of radiation dose. *Journal of Radioanalytical and Nuclear Chemistry* **270,** 413-416.

Tanir, G., Bolukdemir, M. H., Catli, S., and Tel, E. (2007). IRSL characteristics of NaCl and KCl relative to dosimeter. *Radiation Measurements* **42,** 29-34.

Thakur, V. C., Pandey, A. K., and Suresh, N. (2007). Late Quaternary-Holocene evolution of Dun structure and the Himalayan Frontal Fault zone of the Garhwal Sub-Himalaya, NW India. *Journal of Asian Earth Sciences* **29,** 305-319.

Thompson, C., Rhodes, E., and Croke, J. (2007). The storage of bed material in mountain stream channels as assessed using optically stimulated luminescence dating. *Geomorphology* **83,** 307-321.

Thomsen, K. J., Bøtter-Jensen, L., Denby, P. M., and Murray, A. S. (2006). Luminescence response to irradiation using mini X-ray generators. *Nuclear Instruments and Methods in Physics Research Section B:* **252,** 267-275.

Thomsen, K. J., Murray, A. S., Bøtter-Jensen, L., and Kinahan, J. (2007). Determination of burial dose in incompletely bleached fluvial samples using single grains of quartz. *Radiation Measurements* **42,** 370-379.

Tooth, S., Rodnight, H., Duller, G. A. T., McCarthy, T. S., Marren, P. M., and Brandt, D. (2007). Chronology and controls of avulsion along a mixed bedrock-alluvial river. *Bulletin of the Geological Society of America* **119,** 452-461.

Toyoda, S., Tsukamoto, S., Hameau, S., Usui, H., and Suzuki, T. (2006). Dating of Japanese Quaternary tephras by ESR and luminescence methods. *Quaternary Geochronology* **1,** 320-326.

Tsirliganis, N. C., Polymeris, G. S., Kitis, G., and Pagonis, V. (2007). Dependence of the anomalous fading of the TL and blue-OSL of fluorapatite on the occupancy of the tunnelling recombination sites. *Journal of Luminescence* **126,** 303-308.

Tsukamoto, S., Murray, A. S., Huot, S., Watanuki, T., Denby, P. M., and Botter-Jensen, L. (2007). Luminescence property of volcanic quartz and the use of red isothermal TL for dating tephras. *Radiation Measurements* **42,** 190-197.

Turk, I., Blackwell, B. A. B., Turk, J., and Pflaum, M. (2006). Resultats de l'analyse tomographique informatisee de la plus ancienne flute decouverte a Divje babe I (Slovenie) et sa position chronologique dans le contexte des changements paleoclimatiques et paleoenvironnementaux au cours du dernier glaciaire. *L'Anthropologie* **110,** 293-317.

Twidale, C. R., Bourne, J. A., Spooner, N. A., and Rhodes, E. J. (2007). The age of the palaeodunefield of the northern Murray Basin in South Australia: Preliminary results. *Quaternary International* **166,** 42-48.

Veronese, I., Guzzi, G., Giussani, A., Cantone, M. C., and Ripamonti, D. (2006). Determination of dose rates from natural radionuclides in dental materials. *Journal of Environmental Radioactivity* **91,** 15-26.

Veronese, I., Shved, V., Shishkina, E. A., Giussani, A., and Goksu, H. Y. (2007). Study of dose rate profile at sample disks in a Riso OSL single-grain attachment system. *Radiation Measurements* **42,** 138-143.

Vorona, I. P., Baran, N. P., Ishchenko, S. S., and Rudko, V. V. (2007). Separation of the contributions from gamma- and UV-radiation to the EPR spectra of tooth enamel plates. *Applied Radiation and Isotopes* **65,** 553-556.

Walker, R. T., Bayasgalan, A., Carson, R., Hazlett, R., McCarthy, L., Mischler, J., Molor, E., Sarantsetseg, P., Smith, L., Tsogtbadrakh, B., and Tsolmon, G. (2006). Geomorphology and structure of the Jid right-lateral strike-slip fault in the Mongolian Altay mountains. *Journal of Structural Geology* **28,** 1607-1622.

Wang, X. L., Wintle, A. G., and Lu, Y. C. (2007). Testing a single-aliquot protocol for recuperated OSL dating. *Radiation Measurements* **42,** 380-391.

Wu, X. Z., Liu, W., Gao, X., and Yin, G. M. (2006). Huanglong Cave, a new late Pleistocene hominid site in Hubei Province, China. *Chinese Science Bulletin* **51,** 2493-2499.

Xu, S. J., Pan, B. T., Gao, H. S., Cao, G. J., and Su, H. (2007). Changes in sand fractions of Binggou section and the expansion and contraction of the Tengger Desert during 50-30 ka. *Earth Surface Processes and Landforms* **32,** 475-480.

Yawata, T., Hashimoto, T., Takeuchi, T., and Hong, D. G. (2007). Optimal conditions of X-ray irradiation for accurate equivalent dose determination. *Nuclear Instruments and Methods in Physics Research Section B: Beam Interactions with Materials and Atoms* **258,** 375-380.

LED2005 published papers in Quaternary Geochronology (February 2007)

Alexanderson, H., and Murray, A. S. (2007). Was southern Sweden ice free at 19-25 ka, or were the post LGM glacifluvial sediments incompletely bleached? *Quaternary Geochronology* **2,** 229-236.

Almond, P. C., Shanhun, F. L., Rieser, U., and Shulmeister, J. (2007). An OSL, radiocarbon and tephra isochron-based chronology for Birdlings Flat loess at Ahuriri Quarry, Banks Peninsula, Canterbury, New Zealand. *Quaternary Geochronology* **2,** 4-8.

Armitage, S. J., Drake, N. A., Stokes, S., El-Hawat, A., Salem, M. J., White, K., Turner, P., and McLaren, S. J. (2007). Multiple phases of North African humidity recorded in lacustrine sediments from the Fazzan Basin, Libyan Sahara. *Quaternary Geochronology* **2,** 181-186.

Arnold, L. J., Bailey, R. M., and Tucker, G. E. (2007). Statistical treatment of fluvial dose distributions from southern Colorado arroyo deposits. *Quaternary Geochronology* **2,** 162-167.

Bateman, M. D., Boulter, C. H., Carr, A. S., Frederick, C. D., Peter, D., and Wilder, M. (2007). Detecting post-depositional sediment disturbance in sandy deposits using optical luminescence. *Quaternary Geochronology* **2,** 57-64.

Boe, A.-G., Murray, A., and Dahl, S. O. (2007). Resetting of sediments mobilised by the LGM ice-sheet in southern Norway. *Quaternary Geochronology* **2,** 222-228.

Boulter, C., Bateman, M. D., and Frederick, C. D. (2007). Developing a protocol for selecting and dating sandy sites in East Central Texas: Preliminary results. *Quaternary Geochronology* **2,** 45-50.

Bubenzer, O., Hilgers, A., and Riemer, H. (2007). Luminescence dating and archaeology of Holocene fluvio-lacustrine sediments of Abu Tartur, Eastern Sahara. *Quaternary Geochronology* **2,** 314-321.

Buylaert, J. P., Vandenberghe, D., Murray, A. S., Huot, S., De Corte, F., and Van den Haute, P. (2007). Luminescence dating of old (>70 ka) Chinese loess: A comparison of single-aliquot OSL and IRSL techniques. *Quaternary Geochronology* **2,** 9-14.

Cheong, C. S., Choi, J. H., Sohn, Y. K., Kim, J. C., and Jeong, G. Y. (2007). Optical dating of hydromagmatic volcanoes on the southwestern coast of Jeju Island, Korea. *Quaternary Geochronology* **2,** 266-271.

DeLong, S. B., and Arnold, L. J. (2007). Dating alluvial deposits with optically stimulated luminescence, AMS 14C and cosmogenic techniques, western Transverse Ranges, California, USA. *Quaternary Geochronology* **2,** 129-136.

Fiebig, M., and Preusser, F. (2007). Investigating the amount of zeroing in modern sediments of River Danube, Austria. *Quaternary Geochronology* **2,** 143-149.

Fuchs, M., Woda, C., and Burkert, A. (2007). Chronostratigraphy of a sediment record from the Hajar mountain range in north Oman: Implications for optical dating of insufficiently bleached sediments. *Quaternary Geochronology* **2,** 202-207.

Gemmell, A. M. D., Murray, A. S., and Connell, E. R. (2007). Devensian glacial events in Buchan (NE Scotland): A progress report on new OSL dates and their implications. *Quaternary Geochronology* **2,** 237-242.

Jeong, G. Y., Cheong, C.-S., and Choi, J.-H. (2007). The effect of weathering on optically stimulated luminescence dating. *Quaternary Geochronology* **2,** 117-122.

Kortekaas, M., Murray, A. S., Sandgren, P., and Bjorck, S. (2007). OSL chronology for a sediment core from the southern Baltic Sea: A continuous sedimentation record since deglaciation. *Quaternary Geochronology* **2,** 95-101.

Lehmkuhl, F., Zander, A., and Frechen, M. (2007). Luminescence chronology of fluvial and aeolian deposits in the Russian Altai (Southern Siberia). *Quaternary Geochronology* **2,** 195-201.

Li, S.-H., Chen, Y.-Y., Li, B., Sun, J., and Yang, L.-R. (2007). OSL dating of sediments from deserts in northern China. *Quaternary Geochronology* **2,** 23-28.

Lomax, J., Hilgers, A., Twidale, C. R., Bourne, J. A., and Radtke, U. (2007). Treatment of broad palaeodose distributions in OSL dating of dune sands from the western Murray Basin, South Australia. *Quaternary Geochronology* **2,** 51-56.

Lopez, G. I., and Rink, W. J. (2007). Characteristics of the burial environment related to quartz SAR-OSL dating at St. Vincent Island, NW Florida, USA. *Quaternary Geochronology* **2,** 65-70.

Lukas, S., Spencer, J. Q. G., Robinson, R. A. J., and Benn, D. I. (2007). Problems associated with luminescence dating of Late Quaternary glacial sediments in the NW Scottish Highlands. *Quaternary Geochronology* **2,** 243-248.

Madsen, A. T., Murray, A. S., Andersen, T. J., and Pejrup, M. (2007). Optical dating of young tidal sediments in the Danish Wadden Sea. *Quaternary Geochronology* **2,** 89-94.

Mahan, S. A., and Brown, D. J. (2007). An optical age chronology of late Quaternary extreme fluvial events recorded in Ugandan dambo soils. *Quaternary Geochronology* **2,** 174-180.

Mercier, N., Wengler, L., Valladas, H., Joron, J. L., Froget, L., and Reyss, J. L. (2007). The Rhafas Cave (Morocco): Chronology of the mousterian and aterian archaeological occupations and their implications for Quaternary geochronology based on luminescence (TL/OSL) age determinations. *Quaternary Geochronology* **2,** 309-313.

Molodkov, A. (2007). IR-OSL dating of uranium-rich deposits from the new late Pleistocene section at the Voka site, North-Eastern Estonia. *Quaternary Geochronology* **2,** 208-215.

Murray, A. S., Svendsen, J. I., Mangerud, J., and Astakhov, V. I. (2007). Testing the accuracy of quartz OSL dating using a known-age Eemian site on the river Sula, northern Russia. *Quaternary Geochronology* **2,** 102-109.

Narama, C., Kondo, R., Tsukamoto, S., Kajiura, T., Ormukov, C., and Abdrakhmatov, K. (2007). OSL dating of glacial deposits during the Last Glacial in the Terskey-Alatoo Range, Kyrgyz Republic. *Quaternary Geochronology* **2,** 249-254.

Packman, S. C., Mauz, B., Rousseau, D. D., Antoine, P., Rossignol, J., and Lang, A. (2007). Implications of broad dose distributions obtained with the single-aliquot regenerative-dose method on quartz fine-grains from loess. *Quaternary Geochronology* **2,** 39-44.

Porat, N., Levi, T., and Weinberger, R. (2007). Possible resetting of quartz OSL signals during earthquakes--Evidence from late Pleistocene injection dikes, Dead Sea basin, Israel. *Quaternary Geochronology* **2,** 272-277.

Prescott, J. R., Williams, F. M., and Hunt, C. D. (2007). Comparison of TL multiple aliquot, single grain GLSL SAR and C-14 ages for the Puritjarra, Australia, rock shelter. *Quaternary Geochronology* **2,** 344-349.

Sanderson, D. C. W., Bishop, P., Stark, M., Alexander, S., and Penny, D. (2007). Luminescence dating of canal sediments from Angkor Borei, Mekong Delta, Southern Cambodia. *Quaternary Geochronology* **2,** 322-329.

Shen, Z., Mauz, B., Lang, A., Bloemendal, J., and Dearing, J. (2007). Optical dating of Holocene lake sediments: Elimination of the feldspar component in fine silt quartz samples. *Quaternary Geochronology* **2,** 150-154.

Stevens, T., Armitage, S. J., Lu, H., and Thomas, D. S. G. (2007). Examining the potential of high sampling resolution OSL dating of Chinese loess. *Quaternary Geochronology* **2,** 15-22.

Thamo-Bozso, E., Murray, A. S., Nador, A., Magyari, A., and Babinszki, E. (2007). Investigation of river network evolution using luminescence dating and heavy mineral analysis of Late-Quaternary fluvial sands from the Great Hungarian Plain. *Quaternary Geochronology* **2,** 168-173.

Thomas, P. J., Reddy, D. V., Kumar, D., Nagabhushanam, P., Sukhija, B. S., and Sahoo, R. N. (2007). Optical dating of liquefaction features to constrain prehistoric earthquakes in Upper Assam, NE India--some preliminary results. *Quaternary Geochronology* **2,** 278-283.

Thompson, J., Rink, W. J., and Lopez, G. I. (2007). Optically stimulated luminescence age of the Old Cedar midden, St. Joseph Peninsula State Park, Florida. *Quaternary Geochronology* **2,** 350-355.

Wallinga, J., Bos, A. J. J., Dorenbos, P., Murray, A. S., and Schokker, J. (2007). A test case for anomalous fading correction in IRSL dating. *Quaternary Geochronology* **2,** 216-221.

Zander, A., Degering, D., Preusser, F., Kasper, H. U., and Bruckner, H. (2007). Optically stimulated luminescence dating of sublittoral and intertidal sediments from Dubai, UAE: Radioactive disequilibria in the uranium decay series. *Quaternary Geochronology* **2,** 123-128.

Zhang, J.-F., Fan, C.-F., Wang, H., and Zhou, L.-P. (2007). Chronology of an oyster reef on the coast of Bohai Bay, China: Constraints from optical dating using different luminescence signals from fine quartz and polymineral fine grains of coastal sediments. *Quaternary Geochronology* **2,** 71-76.

Zhao, H., Yanchou, L., and Yin, J. (2007). Optical dating of Holocene sand dune activities in the Horqin sand-fields in inner Mongolia, China, using the SAR protocol. *Quaternary Geochronology* **2,** 29-33.

Conference Announcement

UK Luminescence and ESR Meeting

Department of Geography
University of Sheffield

12-14th September 2007

The annual UK Luminescence and ESR dating research meeting will be held at the University of Sheffield from the 12-14th September 2007. This meeting will be of interest to luminescence dating specialists, Quaternary geologists, archaeologists, dosimetric scientists and some physics researchers by providing an opportunity to discuss the latest research in trapped charge dating and related work. Presentations covering basic physics, methodological issues and the application of these techniques are all welcome. The meeting will consist of both oral and poster presentations, and presentations by research students are especially encouraged.

For further information send an e-mail to: Luminescence@sheffield.ac.uk or visit the University of Sheffield Geography department website at http://www.shef.ac.uk/led07 where the Second Circular is now available. Please note that both registration and abstract submission must be completed by the 17th August 2007.

Conference Announcement

Fifth New World Luminescence Dating and Dosimetry Workshop

Department of Earth and Environmental Sciences at the University of Illinois at Chicago

13-14th October 2007

The fifth New World Luminescence Dating and Dosimetry Workshop (NWLDDW) will be held at the Department of Earth and Environmental Sciences at the University of Illinois at Chicago. Workshop presentations are planned for October 13 to 14, 2007 (Saturday and Sunday) at the University of Illinois campus in Chicago. This workshop will gather a diverse group of researchers in Quaternary geology, geomorphology, archaeology, luminescence geochronology, solid-state physics and geochemistry to discuss advances in optical dating and dosimetry. Presentations on the application of techniques, method development, associated physics, and broader geochronologic and dosimetric implications are welcome.

All presentations will be oral. We anticipate two days of presentations and some time for enjoying the University of Illinois campus and the surrounding city. For further information please contact Steve Forman (slf@uic.edu).

Conference Abstracts

Abstracts from the Fourth New World Luminescence Dating Workshop held at the Denver Federal Center, Denver, Colorado, USA between May 31 and June 1, 2006, are now available online. The abstracts in this volume cover OSL methodologies and applications and provide a current synthesis of luminescence work throughout North America. The workshop was sponsored by the U.S. Geological Survey, Crustal Imaging and Characterization Team and North Dakota State University. Participants included thirty-six research scientists and students in geology, archaeology, and physics from the U.S. Geological Survey, Los Alamos National Laboratory, the Kentucky Geological Survey, the Colorado Geological Survey, eight universities in the United States, the University of Quebec (in Montreal, Canada), the Physical Research Laboratory (in Ahmedabad, India) and Risø National Laboratory, Denmark.

The following URL allows anyone who is interested in reading or referencing the abstracts to access the entire report as a PDF.

http://pubs.usgs.gov/of/2006/1351/

Shannon A. Mahan